An Eddy Current and Micromagnetism Model with Applications to Disk Write Heads

J. Sun* F. Collino† P.B. Monk* L. Wang‡

May 28, 2003

Abstract

As data rates increase and the size of the disk write head decreases it is likely that a standard non-linear eddy current simulation of a disk write head will not fully capture dynamic effects. In this paper we propose a coupled eddy-current and micromagnetics model for the disk write head. We present a simple finite difference formulation derived from a mass-lumped finite element method. This derivation allows us to verify that, before time discretization, the semi-discrete scheme obeys the same energy decay equality as the partial differential equation model. We show some numerical results for an "academic" disk writer model.

1 Introduction

The disk write head in a hard disk drive is a small electromagnet (approximately $10\mu\text{m}\times1\mu\text{m}\times0.1\mu\text{m}$). Current through a coil wrapped around the yoke causes an intense magnetic field at the tip of the writer which imprints a magnetic field on the platter to store data. The tip is roughly $0.1\mu\text{m}\times0.1\mu\text{m}$. Because of the small size of the tip and the rate at which data is written to the disk, we shall argue that classical non-linear eddy current models or alternatively micromagnetic models based on a quasi-static demagnetising field may not be sufficient. We therefore propose to use a combined eddy-current and micromagnetic model to provide a novel method for simulating the disk writer.

In evaluating the suitability of a model for the disk write head we can first consider the characteristic time scales for various processes in the model. In this discussion we take the rise time of the current in the coil, denoted by $t_{coil} \approx 0.4$ nanoseconds as a representative time-scale for modelling the writer, and as a representative length scale $L \approx 10^{-6}$m. The most general partial differential equation model of this process is perhaps the coupled system of Maxwell's equations and the Landau-Lifschitz-Gilbert (LLG) equation of micromagnetism [11, 4, 20, 15, 19]. If we then consider the time-scale for electromagnetic wave propagation across the domain we find that $L/(ct_{coil}) \approx 10^{-6}$ where c is the speed of light. Thus we can neglect the displacement current in the Maxwell equations and arrive at the eddy-current model. It is then reasonable to ask if this can be further simplified to a quasi-static model as is usual in micro-magnetic simulations. If we consider the time-scale for diffusion of the electromagnetic field via the Joule effect in the eddy current model, denoted by t_σ, and assume the use of permalloy, we see that

$$t_\sigma = \sigma\mu_0 L^2 \approx 1 \text{ nanosecond}$$

*Department of Mathematical Sciences, University of Delaware, Newark, DE 19716, USA.
†CERFACS, Toulouse, France
‡Seagate Technology, Minneapolis, USA.

This is a similar time-scale to the coil rise-time and thus eddy-currents may have an effect on the behaviour of the electromagnet. This is the reason that a standard nonlinear eddy current model is often used to model the writer. Now considering the LLG equation, and assuming a typical value for the magnetic field due to the coil of 10^4 Oersted we can see that the time-scale for micromagnetic fluctuations given by $t_{llg} = 1/(\gamma|H|)$ where H is the magnitude of the effective field and γ is the gyromagnetic ratio is $t_{llg} \approx 10^{-11}$ seconds. While this is very fast in comparison to the eddy current time-scale, the small dimensions of the tip suggest that micromagnetic effects may influence the behaviour of the writer. Therefore we need to follow the LLG equation in time to obtain the magnetisation (the static LLG system is not easy to solve). Note that the eddy current LLG model has also been investigated for thin films in [16, 10, 2].

A typical academic model of the disk write head is shown in Fig. 1. The inverted U shaped writer yoke (termed the "perpendicular write head" for the remainder of the paper) is shown above the plane of the platter. Because of the desire to write using vertical polarisation of the magnetic field, the plane below the writer has a very high magnetic permeability. The problem we are interested in obtaining the magnetic field under the tip (thin part) of the yoke.

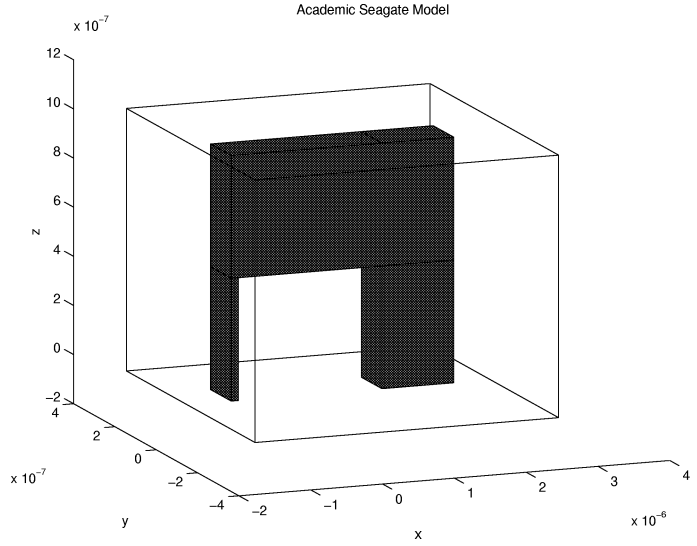

Figure 1: Academic Seagate model. A diagram showing a model simplified perpendicular write head. The ferromagnet occupies the inverted U shaped region shaded in the figure. The lower surface of the computational domain has a very high magnetic permeability. The artificial computational domain Ω is the larger parallelepiped shown.

In most micromagnetic simulations the LLG equation is coupled to a scalar potential equation for the demagnetising field. This system has received a great deal of attention and can be solved by a variety of schemes including coupled integral equation/LLG formulations using multipole methods [12] and finite element formulations [23, 9, 8]. At the other extreme the full Maxwell-LLG model has been considered by a number of authors [19, 15]. The coupled eddy current and LLG model has been used in [16, 10, 2] to model thin films. We use the same time discretization for the LLG equation as was used in [19] and in [16, 10, 2]. However we use a magnetic vector potential for the eddy current solver, allow a non-uniform mesh and take into account the coil. Note that if the exchange contribution is

not present another time integration scheme based on exact integration of the LLG equation has been presented in [17]. One could also perhaps use a projection scheme as in [15, 21, 7].

Finally the mathematical underpinnings of the basic Maxwell-LLG model (and the eddy current-LLG model) are not complete. In a special degenerate case Alouges and Soyeur [1] have demonstrated non-uniqueness in the solution.

2 Eddy Current - LLG Model

The problem is to compute the magnetic induction in a ferromagnetic medium, located above a ground plane of infinite permeability (modelling the high permeability material below the platter), and reacting to some applied field arising from a coil surrounding it. The ferromagnetic medium is located in a bounded subdomain of the half space $\mathbb{R}^3_+$ denoted by

$$\Omega_{\text{ferro}} \subset \mathbb{R}^3_+ = \left\{ \boldsymbol{x} = (x, y, z) \in \mathbb{R}^3,\ z > 0 \right\}.$$

The ferromagnet is assumed to have a nonzero conductivity denoted by σ_{ferro}. We define the global conductivity σ by

$$\sigma(\boldsymbol{x}) = \begin{cases} \sigma_{\text{ferro}}, & \text{if } \boldsymbol{x} \in \Omega_{\text{ferro}}, \\ 0 & \text{elsewhere.} \end{cases}$$

The unknowns of the problems are, as usual for a micromagnetic problem,

$\boldsymbol{E}$, the electric field	$\boldsymbol{B}$, the magnetic induction
$\boldsymbol{M}$, the magnetization	$\boldsymbol{H}$, the magnetic field

where each field is a function of position $\boldsymbol{x}$ and time t.

Outside the ferromagnet (in $\mathbb{R}^3_+ \backslash \overline{\Omega}_{\text{ferro}}$) the magnetization field $\boldsymbol{M} = 0$ and inside the ferromagnet (in Ω_{ferro}) we have $\boldsymbol{M} \neq 0$. Suppose a current $\boldsymbol{J}_{\text{app}}$ due to the coil and supported outside the ferromagnet is applied to the system. The resulting fields are governed by the eddy current equations in $\mathbb{R}^3_+$ for time $t > 0$

$$\begin{cases} \sigma \boldsymbol{E} - \nabla \times \boldsymbol{H} = -\boldsymbol{J}_{\text{app}}, \\ \dfrac{\partial}{\partial t} \boldsymbol{B} + \nabla \times \boldsymbol{E} = 0, \\ \nabla \cdot \boldsymbol{B} = 0, \end{cases} \tag{1}$$

coupled with an appropriate model for the ferromagnet. As discussed in the introduction, we use the Laudau-Lifschitz-Gilbert (LLG) model of micro-magnetism in the ferromagnet Ω_{ferro}. Thus the magnetic induction $\boldsymbol{B}$ is written in terms of the magnetic field $\boldsymbol{H}$ and magnetisation $\boldsymbol{M}$ via

$$\boldsymbol{B} = \mu_0(\boldsymbol{H} + \boldsymbol{M}) \tag{2}$$

and the magnetisation $\boldsymbol{M}$ satisfies the LLG equation.

$$\frac{\partial \boldsymbol{M}}{\partial t} = \gamma \boldsymbol{H}_{\text{eff}} \times \boldsymbol{M} + \alpha \frac{\boldsymbol{M}}{|\boldsymbol{M}|} \times \frac{\partial \boldsymbol{M}}{\partial t} \quad \text{in } \Omega_{\text{ferro}} \tag{3}$$

where $\boldsymbol{H}_{\text{eff}}$ is the effective field, γ is the electron gyromagnetic ratio, and α is the damping constant. In our model, we take the effective field to have three components due respectively to the demagnetizing field, exchange energy and energy of anisotropy. This gives

$$\boldsymbol{H}_{\text{eff}} = \frac{1}{\mu_0} \boldsymbol{B} + \frac{2a}{\mu_0} \Delta \boldsymbol{M} - \frac{2k}{\mu_0} \boldsymbol{P}(\boldsymbol{M}), \tag{4}$$

where a is a phenomenological constant describing the exchange contribution and $\boldsymbol{P}(\boldsymbol{M}) = \boldsymbol{M} - (\boldsymbol{p} \cdot \boldsymbol{M})\boldsymbol{p}$, so that $\boldsymbol{P}(\boldsymbol{M})$ denotes the projection of $\boldsymbol{M}$ on the plane perpendicular to the fixed easy axis $\boldsymbol{p}$ of the uniaxial ferromagnet ($|\boldsymbol{p}| = 1$). The coefficient k gives the strength of the anisotropy contribution. When $a \neq 0$ we also have the boundary condition

$$\frac{\partial \boldsymbol{M}}{\partial \nu} = 0 \text{ on } \partial\Omega_{\text{ferro}}. \tag{5}$$

It is well-known that the magnetisation $\boldsymbol{M}$ satisfies the pointwise conservation equality

$$|\boldsymbol{M}(\boldsymbol{x}, t)| = |\boldsymbol{M}(\boldsymbol{x}, 0)| \quad \text{for all } \boldsymbol{x} \in \Omega \tag{6}$$

as can be seen by taking the dot product of the LLG equation (3) with $\boldsymbol{M}$ and integrating in time. Thus the initial distribution of magnetisation determines $|\boldsymbol{M}|$ for later times.

System (1)-(4) holds for $\boldsymbol{x} = (x, y, z)^T \in \mathbb{R}^3_+$ at $t > 0$. If $\partial\mathbb{R}^3_+ = \{\boldsymbol{x} \in \mathbb{R}^3,\, z = 0\}$, the boundary conditions on the infinitely permeable ground plane $\partial\mathbb{R}^3_+$ is

$$\hat{\boldsymbol{z}} \times (\boldsymbol{H} \times \hat{\boldsymbol{z}}) = 0. \tag{7}$$

This magnetic wall condition arises because the magnetic recording medium is bounded by a layer of very high permeability material. In other directions, the fields remain bounded as $|\boldsymbol{x}| \to \infty$. However, in practice, we shall truncate $\mathbb{R}^3_+$ and compute on a bounded domain Ω. Thus, from now on, we assume that the equations are to be solved on Ω which is taken large enough to contain Ω_{ferro} in its interior. For this paper Ω will be a rectangular parallelepiped given by

$$\Omega = (x^-, x^+) \times (y^-, y^+) \times (0, z^+). \tag{8}$$

After we have reformulated the equations, we shall detail the boundary conditions used on the boundaries of Ω other than the ground plane $\partial\mathbb{R}^3_+$ where $z = 0$. The parallelepiped must be chosen large enough to contain Ω_{ferro} and large enough (by trial and error) that the field at the tip is not influenced appreciably by the choice of Ω_{ferro}.

We would like to use initial data corresponding to a ferromagnetic equilibrium. But this would require to solve the static LLG equation which is a difficult problem [5]. Instead, we assume that at time $t = 0$, the magnetisation field is given by a function $\boldsymbol{M}_0$ so that

$$\boldsymbol{M}(\boldsymbol{x}, t = 0) = \boldsymbol{M}_0(\boldsymbol{x}) \neq 0 \quad \text{in } \Omega_{\text{ferro}},$$

and so that $\boldsymbol{M}_0 = 0$ in $\Omega \setminus \Omega_{\text{ferro}}$. We also assume that no electric field exists at $t = 0$ so

$$\boldsymbol{E}(\boldsymbol{x}, t = 0) = 0 \quad \text{in } \Omega.$$

In order to have a consistent set of initial conditions that satisfy the divergence condition in (1), we need

$$\boldsymbol{B}(\boldsymbol{x}, t = 0) = \boldsymbol{B}_0(\boldsymbol{x}), \quad \boldsymbol{H}(\boldsymbol{x}, t = 0) = \boldsymbol{H}_0(\boldsymbol{x}) \text{ in } \Omega,$$

and $\boldsymbol{B}_0$ and $\boldsymbol{H}_0$ must satisfy the electromagnetic balance laws in Ω so that

$$\begin{cases} \boldsymbol{B}_0 = \mu_0(\boldsymbol{M}_0 + \boldsymbol{H}_0), \\ \nabla \cdot \boldsymbol{B}_0 = 0, \\ \nabla \times \boldsymbol{H}_0 = 0. \end{cases} \tag{9}$$

Thus, the splitting

$$\boldsymbol{M}_0 = \frac{1}{\mu_0}\boldsymbol{B}_0 - \boldsymbol{H}_0,$$

corresponds to a Helmholtz decomposition of $\boldsymbol{M}_0$ (i.e. a decomposition into a divergence free field plus a curl free field). To compute $\boldsymbol{H}_0$ we are led to define $Q_0 = Q_0(\boldsymbol{x})$ as the solution of

$$\begin{cases} \Delta Q_0 = -\nabla \cdot \boldsymbol{M}_0 \quad \text{in } \Omega, \\ \\ Q_0 = 0 \quad \text{on } \partial\Omega, \end{cases} \tag{10}$$

and to set $\boldsymbol{M}_0^{\text{div free}} = \boldsymbol{M}_0 + \nabla Q_0$. Now, it is clear that (9) will hold if we choose $\boldsymbol{H}_0 = \nabla Q_0$ and

$$\boldsymbol{B}_0 = \mu_0\, \boldsymbol{M}_0^{\text{div free}} \tag{11}$$

The field $\boldsymbol{H}_0$ is often referred to as the demagnetization field in classical micromagnetic simulation. We describe $\boldsymbol{B}$ as the demagnetizing field in the eddy current model due to the above connection with the classical field. Note that the boundary conditions and assumption on $\boldsymbol{M}_0$ imply that $\boldsymbol{\nu} \times \boldsymbol{M}_0^{\text{div free}} = 0$ on $\partial\Omega$ where $\boldsymbol{\nu}$ is the unit outward normal.

The applied current $\boldsymbol{J}_{\text{app}}$ is due to the coils. We use a very simple model for the coil that should be improved in future. We assume that the source $\boldsymbol{J}_{\text{app}}$ is due to a line current source with a current $I(t)$ flowing alone the curve denoted $C\text{oil}$. Using the Biot-Savart law this line current creates a magnetic vector potential $\boldsymbol{A}_s = I(t)\boldsymbol{a}_s(\boldsymbol{x})$ (in the absence of the ferromagnet and assuming the domain is $\mathbb{R}^3_+$) where

$$\boldsymbol{a}_s(\boldsymbol{x}) = \frac{\mu_0}{4\pi}\left(\int_{C\text{oil}} \frac{d\boldsymbol{s}(\boldsymbol{y})}{|\boldsymbol{x}-\boldsymbol{y}|} + \int_{\mathcal{S}(C\text{oil})} \frac{d\boldsymbol{s}(\boldsymbol{y})}{|\boldsymbol{x}-\boldsymbol{y}|}\right) \tag{12}$$

and where $\mathcal{S}(C\text{oil})$ is the symmetric coil with respect to the plane $z = 0$. The image coil $\mathcal{S}(C\text{oil})$ ensures that the field due to the coil satisfies the boundary condition (7).

In order to solve the eddy current problem in a convenient way, we define the magnetic vector potential

$$\boldsymbol{A}(\boldsymbol{x}, t) = \int_0^t \boldsymbol{E}(\boldsymbol{x}, \tau)\, d\tau - I(t)\, \boldsymbol{a}_s(\boldsymbol{x}).$$

where $\boldsymbol{a}_s(\boldsymbol{x})$ is the potential due to the coil given above.

Ampere's law, $\partial\boldsymbol{B}/\partial t = -\nabla \times \boldsymbol{E}$, is transformed into

$$\boldsymbol{B} = \boldsymbol{B}_0 - \nabla \times (\boldsymbol{A} + I(t)\boldsymbol{a}_s)\,, \tag{13}$$

where $\boldsymbol{B}_0$ is the magnetic induction at time $t = 0$ given by (11). Furthermore

$$\boldsymbol{H} = \frac{1}{\mu_0}\boldsymbol{B}_0 - \frac{1}{\mu_0}\nabla \times (\boldsymbol{A} + I(t)\boldsymbol{a}_s) - \boldsymbol{M}$$

or, using (11),

$$\boldsymbol{H} = \boldsymbol{M}_0^{\text{div free}} - \frac{1}{\mu_0}\nabla \times (\boldsymbol{A} + I(t)\boldsymbol{a}_s) - \boldsymbol{M}. \tag{14}$$

Using the vector potential $\boldsymbol{A}$, the first equation in (1) is transformed into

$$\begin{aligned} \sigma\frac{\partial}{\partial t}\left(\boldsymbol{A} + I(t)\, \boldsymbol{a}_s\right) \quad &- \quad \nabla \times \left(\boldsymbol{M}_0^{\text{div free}} - \frac{1}{\mu_0}\nabla \times (\boldsymbol{A} + I(t)\boldsymbol{a}_s) - \boldsymbol{M}\right) \\ &= \quad -\boldsymbol{J}_{\text{app}}, \end{aligned}$$

and futhermore

$$\boldsymbol{J} = -I(t)\,\nabla \times \left(\frac{1}{\mu_0}\nabla \times \boldsymbol{a}_s\right).$$

Thus equation (1) implies that

$$\sigma\frac{\partial}{\partial t}\boldsymbol{A} + \nabla \times \left(\frac{1}{\mu_0}\nabla \times \boldsymbol{A}\right) = -\sigma\frac{dI}{dt}(t)\,\boldsymbol{a}_s - \nabla \times \left(\boldsymbol{M} - \boldsymbol{M}_0^{\text{div free}}\right). \tag{15}$$

Our goal is to discretize in space in a way that preserves the conservation of the norm of $\boldsymbol{M}$ given in (6) and preserves a suitable electromagnetic energy that we shall derive shortly. The discretization is based on a variational formulation for the eddy current LLG equations that will provide the basis for our FDTD method via an intermediate finite element discretization. To simplify notation, let $\mathcal{M} = \boldsymbol{M} - \boldsymbol{M}_0^{\text{div free}}$ and $\boldsymbol{A}_s = I(t)\boldsymbol{a}_s$, then we seek a variational formulation for

$$\sigma\frac{\partial \boldsymbol{A}}{\partial t} + \nabla \times \left(\frac{1}{\mu_0}\nabla \times \boldsymbol{A}\right) = -\nabla \times \mathcal{M} - \sigma\frac{\partial}{\partial t}\boldsymbol{A}_s. \tag{16}$$

Equation (16) is posed in the bounded domain $\Omega = (x^-, x^+) \times (y^-, y^+) \times (0, z^+)$ containing the ferro-magnet in it's interior. On the faces of $\partial\Omega$ where $z > 0$ we impose

$$\boldsymbol{A} \times \boldsymbol{\nu} = 0, \tag{17}$$

where $\boldsymbol{\nu}$ is the unit outward normal. On the surface $z = 0$ we impose (7) via

$$(\nabla \times \boldsymbol{A}) \times \boldsymbol{\nu} = 0. \tag{18}$$

To complete the problem, we assume $\boldsymbol{A} = 0$ at $t = 0$ and $\boldsymbol{M}$ is a given function at $t = 0$ in the way described previously.

The space for $\boldsymbol{A}$ is thus

$$X = \{\boldsymbol{u} \in H(\text{curl}; \Omega) \mid \boldsymbol{u} \times \boldsymbol{\nu} = 0 \text{ on all faces of } \Omega \text{ with } z > 0\},$$

where $H(\text{curl}; \Omega)$ is the space of functions in $(L^2(\Omega))^3$ having curl in $(L^2(\Omega))^3$ as usual for electromagnetic problems. Using this space the variational formulation is classical and for a final time $t = T$ is just the problem of finding $\boldsymbol{A} \in C^1(0, T; (L^2(\Omega))^3) \cap C(0, T; X)$ such that

$$\begin{aligned} \int_\Omega \sigma\frac{\partial}{\partial t}\boldsymbol{A} \cdot \boldsymbol{\phi}\, dV \quad &+ \quad \int_\Omega \frac{1}{\mu_0}\nabla \times \boldsymbol{A} \cdot \nabla \times \boldsymbol{\phi}\, dV \\ &= \quad -\int_\Omega \sigma\frac{\partial}{\partial t}\boldsymbol{A}_s \cdot \boldsymbol{\phi}\, dV - \int_\Omega \mathcal{M} \cdot \nabla \times \boldsymbol{\phi}\, dV, \end{aligned} \tag{19}$$

for all $\boldsymbol{\phi} \in X$. Note that the curl has been moved from $\mathcal{M}$ to the test function so this formulation is well defined for $\mathcal{M} \in (L^2(\Omega))^3$. This integration by parts is justified since $\boldsymbol{M}$ vanishes on the surface of Ω by assumption, and $\boldsymbol{M}_0^{\text{div free}}$ has vanishing tangential component on $\partial\Omega$. The LLG equation is then satisfied pointwise in Ω_{ferro} so we assume that $\boldsymbol{M} \in C^1(0, T; (L^\infty(\Omega_{\text{ferro}}))^3) \cap C(0, T; (H^1(\Omega_{\text{ferro}}))^3)$ as required for the upcoming conservation result.

Of course the potential $\boldsymbol{A}$ is not completely determined by the above equations since the divergence of the field is not specified. Since only the curl of $\boldsymbol{A}$ appears in the LLG equation this is not a problem, but it can cause difficulties with the numerical solution [6].

We now derive an energy equality for the eddy current LLG system. For simplicity we shall assume that $I(t) = 0$. Choosing $\boldsymbol{\phi} = \boldsymbol{A}_t = \partial\boldsymbol{A}/\partial t$ in (19) we obtain

$$\int_\Omega \sigma \boldsymbol{A}_t \cdot \boldsymbol{A}_t\, dV = \int_\Omega \mu_0 \boldsymbol{H} \cdot (1/\mu_0)\nabla \times \boldsymbol{A}_t\, dV.$$

where $\boldsymbol{H} = \boldsymbol{M}_0^{\text{div free}} - \boldsymbol{M} - (1/\mu_0)\nabla \times \boldsymbol{A}$ since $I = 0$. Expanding the right hand side we obtain

$$\int_\Omega \sigma \boldsymbol{A}_t \cdot \boldsymbol{A}_t \, dV = -\int_\Omega \mu_0 \boldsymbol{H} \cdot \boldsymbol{H}_t \, dV - \int_\Omega \mu_0 \boldsymbol{H} \cdot \boldsymbol{M}_t \, dV$$

where we have used the boundary condition (5). Now using the definition of the effective field

$$\begin{aligned} \int_\Omega \sigma \boldsymbol{A}_t \cdot \boldsymbol{A}_t \, dV &+ \int_\Omega \mu_0 \boldsymbol{H} \cdot \boldsymbol{H}_t \, dV \\ &= -\int_\Omega \mu_0 \boldsymbol{H}_{\text{eff}} \cdot \boldsymbol{M}_t \, dV \\ &\quad -\int_\Omega \mu_0 \left(\frac{2k}{\mu_0} P(\boldsymbol{M}) - \frac{2a}{\mu_0} \Delta \boldsymbol{M} \right) \cdot \boldsymbol{M}_t \, dV. \end{aligned}$$

But using the LLG equation

$$\int_\Omega \mu_0 \boldsymbol{H}_{\text{eff}} \cdot \boldsymbol{M}_t \, dV = \int_\Omega \alpha \mu_0 \left(\boldsymbol{H}_{\text{eff}} \times \frac{\boldsymbol{M}}{|\boldsymbol{M}|} \right) \cdot \boldsymbol{M}_t \, dV = \int_\Omega \frac{\mu_0 \alpha}{\gamma |\boldsymbol{M}|} |\boldsymbol{M}_t|^2 \, dV.$$

In addition,

$$\int_\Omega \mu_0 \left(\frac{2k}{\mu_0} P(\boldsymbol{M}) - \frac{2a}{\mu_0} \Delta \boldsymbol{M} \right) \cdot \boldsymbol{M}_t \, dV = \frac{d}{dt} \left(\int_\Omega k |\boldsymbol{P}(\boldsymbol{M})|^2 + a |\nabla \boldsymbol{M}|^2 \right) dV.$$

Thus we have proved the following energy conservation result:

Theorem 1 *Suppose $I = 0$ (the coil current vanishes). Then any sufficiently smooth solution of the eddy-current LLG equation satisfies the energy decay equality:*

$$\begin{aligned} &\frac{d}{dt} \int_\Omega \left(\frac{1}{2} \mu_0 |\boldsymbol{H}|^2 + k |\boldsymbol{P}(\boldsymbol{M})|^2 + a |\nabla \boldsymbol{M}|^2 \right) dV + \int_\Omega \sigma |\boldsymbol{A}_t|^2 \, dV \\ &= -\int_\Omega \frac{\mu_0 \alpha}{\gamma |\boldsymbol{M}|} |\boldsymbol{M}_t|^2 \, dV. \end{aligned} \tag{20}$$

Remark. This theorem shows that in the absence of an applied current the electromagnetic energy

$$\int_\Omega \left(\frac{1}{2} \mu_0 |\boldsymbol{H}|^2 + k |\boldsymbol{P}(\boldsymbol{M})|^2 + a |\nabla \boldsymbol{M}|^2 \right) dV$$

is a non-increasing function of time. We would like the approximate numerical solution to obey a similar relation (at least before time discretization).

3 The Finite Element Spaces

In this section we describe how to discretize the eddy-current and LLG equations in a way to conserve the norm of $\boldsymbol{M}$ and the energy in (20). The resulting method will be a finite difference scheme, but having a choice of stencils that allows us to prove energy conservation. We find this easiest to describe as a mass-lumped finite element method, and this is how our code is implemented. As before we assume that $\Omega = (x^-, x^+) \times (y^-, y^+) \times (0, z^+)$. For the x direction, the mesh is defined through a set of given coordinates

$$x^- = x_0 < x_1 < \ldots < x_{n_x} = x^+. \tag{21}$$

These coordinates are referred to as the integer nodes. From this set, we define the half-integer nodes $x_{\frac{1}{2}}$, $x_{\frac{3}{2}}$, ..., $x_{n_x-\frac{1}{2}}$, with

$$x_{i-\frac{1}{2}} = \frac{1}{2}\left(x_i + x_{i-1}\right),\ i = 1, .., n_x. \tag{22}$$

We then define two mesh widths between two consecutive nodes of same type:

$$\left\{ \begin{array}{lcll} \Delta x_{i-\frac{1}{2}} & = & x_i - x_{i-1}, & i = 1, .., n_x \\ \Delta x_i & = & x_{i+\frac{1}{2}} - x_{i-\frac{1}{2}}, & i = 1, .., n_x - 1 \end{array} \right. \tag{23}$$

Fig. 2 shows the mesh graphically.

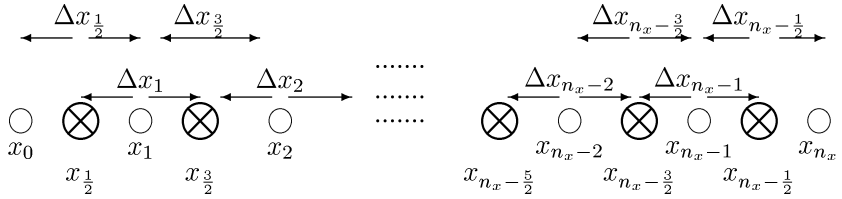

Figure 2: The x-discretization using $n_x + 1$ points. The distance between mesh points does not have to be uniform.

The same definitions relative to the directions y and z give

$$\left\{ \begin{array}{llll} y_{j-\frac{1}{2}}, & y_j, & \Delta y_{j-\frac{1}{2}}, & \Delta y_j, \\ z_{k-\frac{1}{2}}, & z_k, & \Delta z_{k-\frac{1}{2}}, & \Delta z_k. \end{array} \right. \tag{24}$$

These subdivisions induce a meshing of Ω by parallelepipeds

$$\left\{ \begin{array}{l} \overline{\Omega} = \bigcup\limits_{i,j,k} c_{i+\frac{1}{2},j+\frac{1}{2},k+\frac{1}{2}} \\ c_{i+\frac{1}{2},j+\frac{1}{2},k+\frac{1}{2}} = [x_i, x_{i+1}] \times [y_i, y_{i+1}] \times [z_i, z_{i+1}]. \end{array} \right. \tag{25}$$

This will be the mesh for our spatial discretization procedure. Let h denote the maximum mesh width in any of the coordinate directions. We shall use h as a generic symbol for quantities related to the mesh.

We now need to define some basis functions on the mesh. A segment function is a function that is 1 on a segment and 0 elsewhere. For a given direction, a (a can be x, y or z), we define $\psi^{(a)}_{m+\frac{1}{2}}(a)$ the segment function taking the value one only on $[a_m, a_{m+1}]$. In addition, we define the hat function $\phi^{(a)}_m(a)$ as shown next

$\phi^{(a)}_m(a) =$ 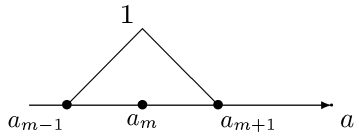

We shall now summarise some properties of appropriate finite element spaces for this problem. These are well known but for completeness we provide explicit constructions of various operators in the case of lowest order Nédélec elements [13].

3.1 The space $\mathcal{H}_h^{\mathrm{curl}} \subset H(\mathrm{curl};\Omega)$

The vector potentials $\boldsymbol{A}$ and $\boldsymbol{A}_s$ are approximated by Nédelec's finite elements of lowest degree [13, 14, 3]. We denote this space by $\mathcal{H}_h^{\mathrm{curl}}$, which is an internal approximation of $H(\mathrm{curl};\Omega)$.

The approximate vector potentials are then given by

$$\begin{aligned} \boldsymbol{A}(\boldsymbol{x},t) &\approx \boldsymbol{A}_h(\boldsymbol{x},t) = \sum_e A_e(t)\,\boldsymbol{\phi}_e^h(\boldsymbol{x}) \\ \boldsymbol{A}_s(\boldsymbol{x},t) &\approx \boldsymbol{A}_{s,h}(\boldsymbol{x},t) = \sum_e (A_s)_e(t)\,\boldsymbol{\phi}_e^h(\boldsymbol{x}) \end{aligned} \tag{26}$$

at every point $\boldsymbol{x}$ in Ω where the functions $\boldsymbol{\phi}_e^h$ are suitable basis functions. For a given edge of the mesh e, the associated basis function has a circulation equal to length(e) for edge e and 0 for the other edges. More precisely, we distinguish edges along the x, y or z directions. Edges are labelled by the coordinates of their middle point. For instance, an edge in x will be associated to a point of type $(x_{i+\frac{1}{2}}, y_j, z_k)$. We are then led to distinguish three families of basis functions

$$\begin{aligned} e = \text{ edge in } x \quad &\rightarrow \quad \boldsymbol{\phi}_e^h = \boldsymbol{\phi}^h_{i+\frac{1}{2},j,k} \\ e = \text{ edge in } y \quad &\rightarrow \quad \boldsymbol{\phi}_e^h = \boldsymbol{\phi}^h_{i,j+\frac{1}{2},k} \\ e = \text{ edge in } z \quad &\rightarrow \quad \boldsymbol{\phi}_e^h = \boldsymbol{\phi}^h_{i,j,k+\frac{1}{2}}, \end{aligned} \tag{27}$$

with

$$\begin{aligned} \boldsymbol{\phi}^h_{i+\frac{1}{2},j,k}(\boldsymbol{x}) &= \psi^{(x)}_{i+\frac{1}{2}}(x)\,\phi^{(y)}_j(y)\,\phi^{(z)}_k(z)\,\hat{\boldsymbol{x}} \\ \boldsymbol{\phi}^h_{i,j+\frac{1}{2},k}(\boldsymbol{x}) &= \psi^{(y)}_{j+\frac{1}{2}}(y)\,\phi^{(z)}_k(z)\,\phi^{(x)}_i(x)\,\hat{\boldsymbol{y}} \\ \boldsymbol{\phi}^h_{i,j,k+\frac{1}{2}}(\boldsymbol{x}) &= \psi^{(z)}_{k+\frac{1}{2}}(z)\,\phi^{(y)}_i(x)\,\phi^{(y)}_j(y)\,\hat{\boldsymbol{z}}, \end{aligned} \tag{28}$$

where $\hat{\boldsymbol{x}}$ is the unit vector along the x axis (and similarly $\hat{\boldsymbol{y}}$ and $\hat{\boldsymbol{z}}$). It is not difficult to see that each basis function is supported by the four cubes sharing the associated edge.

Finally, the vector potential $\boldsymbol{A}_h$ is sought in the form

$$\left\{ \begin{aligned} \boldsymbol{A}_h(\boldsymbol{x},t) = \sum_{i,j,k} & A^x_{i+\frac{1}{2},j,k}(t)\,\boldsymbol{\phi}^h_{i+\frac{1}{2},j,k}(\boldsymbol{x}) + A^y_{i,j+\frac{1}{2},k}(t)\,\boldsymbol{\phi}^h_{i,j+\frac{1}{2},k}(\boldsymbol{x}) \\ & + A^z_{i,j,k+\frac{1}{2}}(t)\,\boldsymbol{\phi}^h_{i,j,k+\frac{1}{2}}(\boldsymbol{x}), \end{aligned} \right. \tag{29}$$

and we have a similar expression for $\boldsymbol{A}_{s,h}$.

Let us remark that the components of the electromagnetic field are exactly the ones that are used for constructing the Yee scheme, [24, 18]. As we shall see, the final method reduces to the Yee scheme for the eddy-current portion of the model on a uniform mesh.

3.2 The space $\mathcal{H}_h^{\mathrm{div}} \subset H(\mathrm{div};\Omega)$

Another space of interest is $\mathcal{H}_h^{\mathrm{div}}$, which is an internal approximation of $H(\mathrm{div};\Omega)$. Every element of this space is written as

$$B^h(\boldsymbol{x}) = \sum_f B_f^h\,\boldsymbol{\psi}_f^h(\boldsymbol{x}), \tag{30}$$

where the functions $\boldsymbol{\psi}_f^h$ are appropriate basis functions. For a given face f, the associated function has an outgoing normal flux across f equal the surface area of f and vanishing on the others faces.

Depending on the orientation of the normal to the faces, three families of basis functions can be distinguished. Each face is labelled by the coordinates of its centre. To a face with normal $\pm\hat{\boldsymbol{x}}$ corresponds a point of type $(x_i, x_{j+\frac{1}{2}}, z_{k+\frac{1}{2}})$. The associated basis functions are then

$$\begin{aligned} f = \text{ face in } x \quad &\rightarrow \quad \boldsymbol{\psi}_f^h = \boldsymbol{\psi}_{i,j+\frac{1}{2},k+\frac{1}{2}}^h, \\ f = \text{ face in } y \quad &\rightarrow \quad \boldsymbol{\psi}_f^h = \boldsymbol{\psi}_{i+\frac{1}{2},j,k+\frac{1}{2}}^h, \\ f = \text{ face in } z \quad &\rightarrow \quad \boldsymbol{\psi}_f^h = \boldsymbol{\psi}_{i+\frac{1}{2},j+\frac{1}{2},k}^h, \end{aligned} \tag{31}$$

with

$$\begin{aligned} \boldsymbol{\psi}_{i,j+\frac{1}{2},k+\frac{1}{2}}^h(\boldsymbol{x}) &= \phi_i^{(x)}(x)\ \psi_{j+\frac{1}{2}}^{(y)}(y)\ \psi_{k+\frac{1}{2}}^{(z)}(z)\ \hat{\boldsymbol{x}} \\ \boldsymbol{\psi}_{i+\frac{1}{2},j,k+\frac{1}{2}}^h(\boldsymbol{x}) &= \phi_j^{(y)}(y)\ \psi_{k+\frac{1}{2}}^{(z)}(z)\ \psi_{i+\frac{1}{2}}^{(x)}(x)\ \hat{\boldsymbol{y}} \\ \boldsymbol{\psi}_{i+\frac{1}{2},j+\frac{1}{2},k}^h(\boldsymbol{x}) &= \phi_k^{(z)}(z)\ \psi_{i+\frac{1}{2}}^{(x)}(x)\ \psi_{j+\frac{1}{2}}^{(y)}(y)\ \hat{\boldsymbol{z}}. \end{aligned} \tag{32}$$

The basis function associated to face f is supported by the two cubes whose one of the faces is f .

3.2.1 The curl operator from $\mathcal{H}_h^{\text{curl}}$ into $\mathcal{H}_h^{\text{div}}$

In our context, an important property of the space $\mathcal{H}_h^{\text{div}}$ is that

$$\nabla\times: \quad \mathcal{H}_h^{\text{curl}} \quad \longrightarrow \quad \mathcal{H}_h^{\text{div}}$$

that is to say the curl of an edge function is a face function (with zero divergence). Thus if the vector potential $\boldsymbol{A}$ is discretized by edge elements in $\mathcal{H}_h^{\text{curl}}$, then the approximate magnetic induction computed from the curl of $\boldsymbol{A}$ will be discretized in $\mathcal{H}_h^{\text{div}}$. To see this, let us compute

$$\left\{ \begin{aligned} \nabla \times \left(\boldsymbol{\phi}_{i+\frac{1}{2},j,k}^h\right)(\boldsymbol{x}) &= \nabla \times \left(\psi_{i+\frac{1}{2}}^{(x)}(x)\,\phi_j^{(y)}(y)\,\phi_k^{(z)}(z)\ \hat{\boldsymbol{x}}\right) \\ &= \psi_{i+\frac{1}{2}}^{(x)}(x)\phi_j^{(y)}(y)\frac{d\phi_k^{(z)}}{dz}(z)\ \hat{\boldsymbol{y}} - \psi_{i+\frac{1}{2}}^{(x)}(x)\frac{d\phi_j^{(y)}}{dy}(y)\,\phi_k^{(z)}(z)\ \hat{\boldsymbol{z}} \\ &= \psi_{i+\frac{1}{2}}^{(x)}(x)\phi_j^{(y)}(y)\frac{-\psi_{k+\frac{1}{2}}^{(z)} + \psi_{k-\frac{1}{2}}^{(z)}}{(\Delta z)_k}(z)\ \hat{\boldsymbol{y}} \\ &\qquad -\psi_{i+\frac{1}{2}}^{(x)}(x)\frac{-\psi_{j+\frac{1}{2}}^{(y)} + \psi_{j-\frac{1}{2}}^{(y)}}{dy}(y)\,\phi_k^{(z)}(z)\ \hat{\boldsymbol{z}} \end{aligned} \right.$$

and so

$$\left\{ \begin{aligned} \nabla \times \left(\boldsymbol{\phi}_{i+\frac{1}{2},j,k}^h\right) = \quad & \frac{\boldsymbol{\psi}_{i+\frac{1}{2},j+\frac{1}{2},k} - \boldsymbol{\psi}_{i+\frac{1}{2},j-\frac{1}{2},k}}{(\Delta y)_j} \\ - \quad & \frac{\boldsymbol{\psi}_{i+\frac{1}{2},j,k+\frac{1}{2}} - \boldsymbol{\psi}_{i+\frac{1}{2},j,k-\frac{1}{2}}}{(\Delta z)_k}. \end{aligned} \right. \tag{33}$$

In the same way, we get

$$\left\{ \begin{aligned} \nabla \times \left(\boldsymbol{\phi}_{i,j+\frac{1}{2},k}^h\right) = \quad & \frac{\boldsymbol{\psi}_{i,j+\frac{1}{2},k+\frac{1}{2}} - \boldsymbol{\psi}_{i,j+\frac{1}{2},k-\frac{1}{2}}}{(\Delta z)_k} \\ - \quad & \frac{\boldsymbol{\psi}_{i+\frac{1}{2},j+\frac{1}{2},k} - \boldsymbol{\psi}_{i-\frac{1}{2},j+\frac{1}{2},k}}{(\Delta x)_i}, \end{aligned} \right. \tag{34}$$

and

$$\left\{ \begin{aligned} \nabla \times \left(\boldsymbol{\phi}_{i,j,k+\frac{1}{2}}\right) = \quad & \frac{\boldsymbol{\psi}_{i+\frac{1}{2},j,k+\frac{1}{2}} - \boldsymbol{\psi}_{i-\frac{1}{2},j,k+\frac{1}{2}}}{(\Delta x)_i} \\ - & \frac{\boldsymbol{\psi}_{i,j+\frac{1}{2},k+\frac{1}{2}} - \quad \boldsymbol{\psi}_{i,j-\frac{1}{2},k+\frac{1}{2}}}{(\Delta y)_j}, \end{aligned} \right. \tag{35}$$

Thus, if $\boldsymbol{A}_h \in \mathcal{H}_h^{\text{curl}}$, we have $\nabla \times \boldsymbol{A}_h \in \mathcal{H}_h^{\text{div}}$. In particular we see that the contribution of the vector potential to $\boldsymbol{B}_h$ is in $\mathcal{H}_h^{\text{div}}$ and so is associated with faces in the mesh.

3.3 The space $\mathcal{H}_h$

The last space we will consider is $\mathcal{H}_h$, the set of piecewise constant functions whose restriction to any cube of the mesh is constant. Elements in this space will be referred to as cube functions. The basis functions are the functions that are 1 on a particular cube and 0 elsewhere. If each cube is labelled by the coordinates of its centre, we have

$$\chi^h_{i+\frac{1}{2},j+\frac{1}{2},k+\frac{1}{2}}(\boldsymbol{x}) = \psi^{(x)}_{i+\frac{1}{2}}(x)\,\psi^{(y)}_{j+\frac{1}{2}}(y)\,\psi^{(z)}_{k+\frac{1}{2}}(z) \tag{36}$$

The space $\mathcal{H}_h$ will be used to discretized the physical parameters of the model, i.e. the conductivity $\sigma(\boldsymbol{x})$ (in this paper the permeability μ is assumed constant since the LLG equation effectively implies a non constant μ). In particular We assume

$$\sigma(\boldsymbol{x}) = \sum_{i,j,k} \sigma_{i+\frac{1}{2},j+\frac{1}{2},k+\frac{1}{2}}\ \chi^h_{i+\frac{1}{2},j+\frac{1}{2},k+\frac{1}{2}}(\boldsymbol{x}). \tag{37}$$

Furthermore, the space $(\mathcal{H}_h)^3$ will be used for approximating each component of the magnetic moment:

$$\mathcal{M}(t) \approx \mathcal{M}_h(t) \in \mathcal{H}_h \times \mathcal{H}_h \times \mathcal{H}_h \tag{38}$$

and

$$\mathcal{M}_h(\boldsymbol{x},t) = \sum_c \mathcal{M}_c(t)\ \chi_c(\boldsymbol{x}) \tag{39}$$

where $\mathcal{M}_c \in \mathbb{R}^3$ or equivalently

$$\mathcal{M}_h(\boldsymbol{x},t) = \sum_{i,j,k} \mathcal{M}_{i+\frac{1}{2},j+\frac{1}{2},k+\frac{1}{2}}(t)\ \ \chi_{i+\frac{1}{2},j+\frac{1}{2},k+\frac{1}{2}}(\boldsymbol{x}). \tag{40}$$

3.3.1 The div operator from $\mathcal{H}_h^{\text{div}}$ into $\mathcal{H}_h$

A useful property of the space $\mathcal{H}_h^{\text{div}}$ is that

$$\nabla\cdot : \quad \mathcal{H}_h^{\text{div}} \quad \longrightarrow \quad \mathcal{H}_h$$

that is to say the divergence of a face function is a cube function. Indeed, it is straightforward to obtain

$$\left\{\begin{array}{l} \nabla\cdot\left(\boldsymbol{\psi}^h_{i,j+\frac{1}{2},k+\frac{1}{2}}\right)(\boldsymbol{x}) = \nabla\cdot\left(\phi^{(x)}_i(x)\,\psi^{(y)}_{j+\frac{1}{2}}(y)\,\psi^{(z)}_{k+\frac{1}{2}}(z)\,\hat{\boldsymbol{x}}\right) \\ \qquad = \dfrac{d\phi^{(x)}_i}{dx}(x)\,\psi^{(y)}_{j+\frac{1}{2}}(y)\,\psi^{(z)}_{k+\frac{1}{2}}(z) = \dfrac{\psi^{(x)}_{i+\frac{1}{2}} - \psi^{(x)}_{i-\frac{1}{2}}}{(\Delta x)_i}\,\psi^{(y)}_{j+\frac{1}{2}}(y)\,\psi^{(z)}_{k+\frac{1}{2}}(z) \end{array}\right.$$

and so

$$\nabla\cdot\left(\boldsymbol{\psi}^h_{i,j+\frac{1}{2},k+\frac{1}{2}}\right) = \frac{\chi_{i-\frac{1}{2},j+\frac{1}{2},k+\frac{1}{2}} - \chi_{i+\frac{1}{2},j+\frac{1}{2},k+\frac{1}{2}}}{(\Delta x)_i} \tag{41}$$

In the same way, it is readily seen that

$$\begin{aligned} \nabla\cdot\left(\boldsymbol{\psi}^h_{i+\frac{1}{2},j,k+\frac{1}{2}}\right) &= \frac{\chi_{i+\frac{1}{2},j-\frac{1}{2},k+\frac{1}{2}} - \chi_{i+\frac{1}{2},j+\frac{1}{2},k+\frac{1}{2}}}{(\Delta y)_j}, \\ \nabla\cdot\left(\boldsymbol{\psi}^h_{i+\frac{1}{2},j+\frac{1}{2},k}\right) &= \frac{\chi_{i+\frac{1}{2},j+\frac{1}{2},k-\frac{1}{2}} - \chi_{i+\frac{1}{2},j+\frac{1}{2},k+\frac{1}{2}}}{(\Delta z)_k}. \end{aligned}$$

4 The semi-discretized problem

The semi-discretized eddy-current problem is obtained by discretizing only in space using $X_h = \mathcal{H}_h^{\text{curl}} \cap X$ in place of X in the eddy current variational formulation. The standard finite element discretization of (19) is thus to find $\boldsymbol{A}_h(t) \in X_h$ such that

$$\begin{aligned}&\int_\Omega \sigma \frac{\partial \boldsymbol{A}_h}{\partial t} \cdot \boldsymbol{\phi}_h \, dV + \int_\Omega \frac{1}{\mu} (\nabla \times \boldsymbol{A}_h) \cdot (\nabla \times \boldsymbol{\phi}_h) \, dV \\ &= -\int_\Omega \sigma \frac{\partial}{\partial t} \boldsymbol{A}_{s,h} \cdot \boldsymbol{\phi}_h dV - \int_\Omega \mathcal{M}_h \cdot \nabla \times \boldsymbol{\phi}_h \, dV. \end{aligned} \tag{42}$$

for all $\boldsymbol{\phi}_h \in X_h$ and $\boldsymbol{A}_{s,h} \in \mathcal{H}_h^{\text{curl}}$ is an approximation to $\boldsymbol{A}_s$. This, however, is not the discrete formulation we wish to use.

In order to derive a finite difference scheme we replace the integrals in this system by a quadrature rule to obtain a mass-lumped system. The advantage of using a quadrature rule in place of exact integration to define the discrete problem is that, if it is appropriately chosen, it further sparsifies the matrices without altering the precision of the method. We choose the quadrature rule in such a way the basic eddy current equations corresponds to the Yee scheme on a uniform grid. In particular, we choose

$$\int_\Omega f(\boldsymbol{x}) \, dV \approx \oint_\Omega f(\boldsymbol{x}) \, dV = \sum_{c=c_{i+\frac{1}{2},j+\frac{1}{2},k+\frac{1}{2}}} \frac{\text{Vol}(c)}{8} \sum_{v \in \mathcal{V}(c)} f_{|_c}(v), \tag{43}$$

where $\mathcal{V}(c)$ are the 8 vertices of cube c and $f_{|_c}$ denotes the restriction of function f to the cube c (this allows us to deal with discontinuous functions either).

Another, more explicit, formula is

$$\oint_\Omega f(\boldsymbol{x}) \, dV = \sum_{i,j,k} (\Delta_x)_{i+\frac{1}{2}} \, (\Delta_y)_{j+\frac{1}{2}} \, (\Delta_z)_{k+\frac{1}{2}} \, f_{i+\frac{1}{2},j+\frac{1}{2},k+\frac{1}{2}} \tag{44}$$

with

$$\left\{ \begin{array}{c} f_{i+\frac{1}{2},j+\frac{1}{2},k+\frac{1}{2}} = \\ \frac{1}{8} \big(\quad f(x_{i,j,k}) + f(x_{i+1,j,k}) + f(x_{i+1,j+1,k}) + f(x_{i,j+1,k+1}) + \\ f(x_{i,j+1,k}) + f(x_{i,j,k+1}) + f(x_{i+1,j,k+1}) + f(x_{i+1,j+1,k+1}) \quad \big) \end{array} \right. \tag{45}$$

(we ought to have written $f_{|c_{i+\frac{1}{2},j+\frac{1}{2},k+\frac{1}{2}}}(x_{....})$ instead of $f(x_{...})$!). It is known that this formula is exact for functions whose restriction to each cube of the mesh is piecewise linear.

An additional complication is that we wish to approximate $\boldsymbol{M}$ by a discrete field $\boldsymbol{M}_h \in (\mathcal{H}_h)^3$. We are then faced with the problem of defining $\Delta \boldsymbol{M}_h$ which is needed for the discrete effective magnetic field $\boldsymbol{H}_{\text{eff},h} \in (\mathcal{H}_h)^3$. We use a mixed method approach equivalent to a block centered finite difference scheme when the mesh is uniform. Suppose $\boldsymbol{\psi} \in (H(\text{div}; \Omega))^3$ (so it is a matrix and each column of the matrix is in $H(\text{div}; \Omega)$) then we denote by $\nabla \cdot \boldsymbol{\psi}$ the vector obtained by taking the divergence of each column of $\boldsymbol{\psi}$ so if $\boldsymbol{\psi} = (\boldsymbol{\psi}_1 | \boldsymbol{\psi}_2 | \boldsymbol{\psi}_3)$ we have $\nabla \cdot \boldsymbol{\psi} = (\nabla \cdot \boldsymbol{\psi}_1 | \nabla \cdot \boldsymbol{\psi}_2 | \nabla \cdot \boldsymbol{\psi}_3)^T$. Suppose $\boldsymbol{v}$ is the 3×3 matrix of gradients of $\boldsymbol{M}$ so that

$$\boldsymbol{v} = \nabla \boldsymbol{M} = (\nabla M_1 | \nabla M_2 | \nabla M_3)$$

then if $\boldsymbol{v}$ is smooth enough, we know that $\Delta \boldsymbol{M} = \nabla \cdot \boldsymbol{v}$.

Our discrete Laplacian is based on these formulae using a variational characterization as follows. Using the fact that the appropriate boundary condition for $\boldsymbol{M}$ on

$\partial\Omega_{\text{ferro}}$ is $\partial \boldsymbol{M}/\partial\nu = 0$ we see that an appropriate space for $\boldsymbol{v}$ is $(H_0(\text{div};\Omega_{\text{ferro}}))^3$ where

$$H_0(\text{div};\Omega_{\text{ferro}}) = \{\boldsymbol{v} \in H(\text{div};\Omega_{\text{ferro}}) \mid \boldsymbol{v}\cdot\boldsymbol{\nu} = 0 \text{ on } \partial\Omega_{\text{ferro}}\}\,.$$

Thus $\boldsymbol{v} \in (H_0(\text{div};\Omega_{\text{ferro}}))^3$ satisfies (using integration by parts)

$$0 = \int_{\Omega_{\text{ferro}}} (\boldsymbol{v}\cdot\boldsymbol{\xi} - \nabla\boldsymbol{M}\cdot\boldsymbol{\xi})\,dV = \int_{\Omega_{\text{ferro}}} (\boldsymbol{v}\cdot\boldsymbol{\xi} + \boldsymbol{M}\cdot(\nabla\cdot\boldsymbol{\xi}))\,dV. \tag{46}$$

for any $\boldsymbol{\xi} \in (H_0(\text{div};\Omega_{\text{ferro}}))^3$ where the dot product is column wise and produces a vector! The above variational formulation allows us to introduce an auxiliary vector representing $\nabla\cdot\boldsymbol{M}$ and hence obtain $\Delta\boldsymbol{M}$ even for discontinuous fields.

One final operator is needed to complete the specification of the semi-discrete system. We define the $(L^2(\Omega))^3$ orthogonal projection P_h onto $\mathcal{H}_h^3$ by

$$P_h:\ \mathcal{H}_h^{\text{div}} \longrightarrow \mathcal{H}_h^3$$

In practice this just means that if $\boldsymbol{w}_h \in \mathcal{H}_h^{\text{div}}$ then $P_h\boldsymbol{w}_h$ is the piecewise constant vector computed by avergaing $\boldsymbol{w}_h$ to the centroid of each element. This is a local operation.

The semi-discrete eddy current–LLG variational problem can be obtained by replacing the integrals in (42) and (46) by the quadrature formula discussed earlier in this section. Let $Y_h = \left(\mathcal{H}_h^{\text{div}} \cap H_0(\text{div};\Omega_{\text{ferro}})\right)^3$. The vector potential $\boldsymbol{A}_h(t) \in X_h$, auxiliary variable $\boldsymbol{v}_h(t) \in Y_h$ and magnetisation $\boldsymbol{M}_h(t) \in \mathcal{H}_h^3$ satisfy

$$\begin{aligned}
\int_\Omega \sigma\frac{\partial}{\partial t}\boldsymbol{A}_h\cdot\boldsymbol{\phi}_h\,dV \quad &+ \quad \int_\Omega \frac{1}{\mu}(\nabla\times\boldsymbol{A}_h)\cdot(\nabla\times\boldsymbol{\phi}_h)\,dV, && (47)\\
&= \quad -\int_\Omega \sigma\frac{\partial}{\partial t}\boldsymbol{A}_{s,h}\cdot\boldsymbol{\phi}_h\,dV - \int_\Omega \mathcal{M}_h\cdot\nabla\times\boldsymbol{\phi}_h\,dV,\\
\boldsymbol{B}_h \quad &= \quad \mu_0\boldsymbol{M}_{0,h}^{\text{div free}} - \nabla\times(\boldsymbol{A}_h + I(t)\boldsymbol{a}_{s,h})\,, && (48)\\
\int_\Omega \left(\boldsymbol{v}_h\cdot\boldsymbol{\psi}_h \quad &+ \quad \boldsymbol{M}_h\cdot(\nabla\cdot\boldsymbol{\psi}_h)\right)dV = 0, && (49)\\
\boldsymbol{H}_{\text{eff,h}} \quad &= \quad \frac{1}{\mu_0}P_h\boldsymbol{B}_h + \frac{2a}{\mu_0}\nabla\cdot\boldsymbol{v}_h - \frac{2k}{\mu_0}\boldsymbol{P}(\boldsymbol{M}_h), && (50)\\
\int_\Omega \frac{\partial}{\partial t}\boldsymbol{M}_h\cdot\boldsymbol{\xi}_h\,dV \quad &= \quad \gamma\int_\Omega \boldsymbol{H}_{\text{eff,h}}\times\boldsymbol{M}_h\cdot\boldsymbol{\xi}_h\,dV\\
&\quad\quad +\alpha\int_\Omega \frac{\boldsymbol{M}_h}{|\boldsymbol{M}_h|}\times\frac{\partial\boldsymbol{M}_h}{\partial t}\cdot\boldsymbol{\xi}_h\,dV, && (51)
\end{aligned}$$

for all $\boldsymbol{\phi}_h \in X_h$, for all $\boldsymbol{\psi}_h \in Y_h$ and for all $\boldsymbol{\xi}_h \in \mathcal{H}_h^3$. In these equations $\mathcal{M}_h = \boldsymbol{M}_h - \boldsymbol{M}_{0,h}^{\text{div free}}$ and $\boldsymbol{M}_{0,h}^{\text{div free}} \in \mathcal{H}_h^{\text{div}}$ is an approximation to $\boldsymbol{M}_0^{\text{div free}}$ that we shall detail shortly. In addition $\boldsymbol{A}_{s,h} = I(t)\boldsymbol{a}_{s,h}$ is an approximation to $\boldsymbol{A}_s$, again detailed shortly.

Let E_I denote the set of edges of the mesh that are not on the boundary surfaces having $z > 0$. Since $\{\boldsymbol{\phi}_e\}_{e\in E_I}$ is a basis for the discretization space X_h, problem (47) is equivalent to finding $\boldsymbol{A}_h \in X_h$ such that

$$\begin{aligned}
&\int_\Omega \sigma\frac{\partial\boldsymbol{A}_h}{\partial t}\cdot\boldsymbol{\phi}_e\,dV + \int_\Omega \frac{1}{\mu}(\nabla\times\boldsymbol{A}_h)\cdot(\nabla\times\boldsymbol{\phi}_e)\,dV && (52)\\
&= -\int_\Omega \sigma\frac{\partial}{\partial t}\boldsymbol{A}_{s,h}\cdot\boldsymbol{\phi}_e dV - \int_\Omega \mathcal{M}_h\cdot(\nabla\times\boldsymbol{\phi}_e)\,dV,
\end{aligned}$$

for all $e \in E_I$. Remembering that

$$\boldsymbol{A}_h(\boldsymbol{x},t) = \sum_{e'\in E_I} A_{e'}(t)\boldsymbol{\phi}_{e'}(\boldsymbol{x}),$$

we obtain the system,

$$\sum_{e' \in E_I} \int_\Omega \sigma \boldsymbol{\phi}_{e'} \cdot \boldsymbol{\phi}_e \, dV \, \frac{dA_{e'}}{dt} + \sum_{e' \in E_I} \int_\Omega \frac{1}{\mu} (\nabla \times \boldsymbol{\phi}_{e'}) \cdot (\nabla \times \boldsymbol{\phi}_e) \, dV \, A_{e'}(t) =$$
$$- \int_\Omega \sigma \frac{\partial}{\partial t} \boldsymbol{A}_{s,h} \cdot \boldsymbol{\phi}_e \, dV - \int_\Omega \mathcal{M}_h \cdot (\nabla \times \boldsymbol{\phi}_e) \, dV,$$

for all $e \in E_I$. Gathering, at each time t, the values of the potential vector at each degree of freedom into a vector $\vec{A}(t)$, a system of ordinary differential equations is obtained so that

$$\boldsymbol{M}_\sigma^h \frac{d\vec{A}}{dt} + \boldsymbol{K}^h \vec{A} = -\vec{F}^h(t). \tag{53}$$

5 Assembly Process

Because we use a lumped finite element description and a non-uniform grid it is convenient to assemble the various finite difference matrices element by element. Here we give the resulting formulae.

5.1 The "pseudo-mass" matrix in $\mathcal{H}_h^{\text{curl}}$

The "pseudo-mass" matrix[1] is defined by

$$\left(\boldsymbol{M}_\sigma^h \right)_{e,e'} = \int_\Omega \sigma(\boldsymbol{x}) \boldsymbol{\phi}_e^h(\boldsymbol{x}) \cdot \boldsymbol{\phi}_{e'}^h(\boldsymbol{x}) \, dV \tag{54}$$

The advantage of the quadrature rule (44)-(45) is that it allows us to obtain a diagonal matrix. We get

$$\left(\boldsymbol{M}_\sigma^h \right)_{e,e'} = \left(\boldsymbol{m}_\sigma^h \right)_e \, \delta_{e,e'} \tag{55}$$

where the diagonal term is given by

$$\left(\boldsymbol{m}_\sigma^h \right)_{i+\frac{1}{2},j,k} = \frac{1}{4} \sum_{\varepsilon_1 = \pm 1} \sum_{\varepsilon_2 = \pm 1} (\Delta_x)_{i+\frac{1}{2}} \, (\Delta_y)_{j+\frac{\varepsilon_1}{2}} \, (\Delta_z)_{k+\frac{\varepsilon_2}{2}} \, \sigma_{i+\frac{1}{2},j+\frac{\varepsilon_1}{2},k+\frac{\varepsilon_2}{2}}, \tag{56}$$

for an edge in the x direction. In the same way we have

$$\left(\boldsymbol{m}_\sigma^h \right)_{i,j+\frac{1}{2},k} = \frac{1}{4} \sum_{\varepsilon_1 = \pm 1} \sum_{\varepsilon_2 = \pm 1} (\Delta_x)_{i+\frac{\varepsilon_1}{2}} \, (\Delta_y)_{j+\frac{1}{2}} \, (\Delta_z)_{k+\frac{\varepsilon_2}{2}} \, \sigma_{i+\frac{\varepsilon_1}{2},j+\frac{1}{2},k+\frac{\varepsilon_2}{2}} \tag{57}$$

$$\left(\boldsymbol{m}_\sigma^h \right)_{i,j,k+\frac{1}{2}} = \frac{1}{4} \sum_{\varepsilon_1 = \pm 1} \sum_{\varepsilon_2 = \pm 1} (\Delta_x)_{i+\frac{\varepsilon_1}{2}} \, (\Delta_y)_{j+\frac{\varepsilon_2}{2}} \, (\Delta_z)_{k+\frac{1}{2}} \, \sigma_{i+\frac{\varepsilon_1}{2},j+\frac{\varepsilon_2}{2},k+\frac{1}{2}} \tag{58}$$

for the directions y and z

5.2 The "mass" matrix in $\mathcal{H}_h^{\text{div}}$

The "mass" matrix is defined by

$$\left(\boldsymbol{M}_{\frac{1}{\mu_0}}^h \right)_{f,f'} = \int_\Omega \frac{1}{\mu_0} \boldsymbol{\psi}_f^h(\boldsymbol{x}) \cdot \boldsymbol{\psi}_{f'}^h(\boldsymbol{x}) \, dV \tag{59}$$

The quadrature rule (44)-(45) again allows us to obtain also a diagonal matrix. We get

$$\left(\boldsymbol{M}_{\frac{1}{\mu_0}}^h \right)_{f,f'} = \left(\boldsymbol{m}_{\frac{1}{\mu_0}}^h \right)_f \, \delta_{f,f'} \tag{60}$$

[1] We call it pseudo because σ can vanish in some place

where the diagonal term is given by

$$\left(\boldsymbol{m}^h_{\frac{1}{\mu_0}}\right)_{i,j+\frac{1}{2},k+\frac{1}{2}} = \frac{1}{2}\sum_{\varepsilon_1=\pm 1}(\Delta_x)_{i+\frac{\varepsilon_1}{2}}\,(\Delta_y)_{j+\frac{1}{2}}\,(\Delta_z)_{k+\frac{1}{2}}\,\frac{1}{\mu_0} \tag{61}$$

for a face perpendicular to the x direction. For the other directions, we get

$$\begin{aligned}\left(\boldsymbol{m}^h_{\frac{1}{\mu_0}}\right)_{i+\frac{1}{2},j,k+\frac{1}{2}} &= \frac{1}{2}\sum_{\varepsilon_1=\pm 1}(\Delta_x)_{i+\frac{1}{2}}\,(\Delta_y)_{j+\frac{\varepsilon_1}{2}}\,(\Delta_z)_{k+\frac{1}{2}}\,\frac{1}{\mu_0},\\ \left(\boldsymbol{m}^h_{\frac{1}{\mu_0}}\right)_{i+\frac{1}{2},j+\frac{1}{2},k} &= \frac{1}{2}\sum_{\varepsilon_1=\pm 1}(\Delta_x)_{i+\frac{1}{2}}\,(\Delta_y)_{j+\frac{1}{2}}\,(\Delta_z)_{k+\frac{\varepsilon_1}{2}}\,\frac{1}{\mu_0}.\end{aligned}$$

5.3 Curl matrix

We define matrix $\mathbf{C^h}$ through

$$\nabla\times\boldsymbol{\phi}_e(\boldsymbol{x}) = \sum_f \boldsymbol{C}^h_{f,e}\boldsymbol{\psi}_f(\boldsymbol{x}). \tag{62}$$

Here, we have used $\boldsymbol{C}^h_{f,e}$ instead of $\boldsymbol{C}^h_{e,f}$ to recover the usual notations of finite differences. According to paragraph 3.2.1, we have

$$\begin{cases}\boldsymbol{C}^h_{(i+\frac{1}{2},j+\frac{\varepsilon}{2},k),\,(i+\frac{1}{2},j,k)} &= \dfrac{\epsilon}{(\Delta y)_j}, \quad \varepsilon=\pm 1,\\ \boldsymbol{C}^h_{(i+\frac{1}{2},j,k+\frac{\varepsilon}{2}),\,(i+\frac{1}{2},j,k)} &= -\dfrac{\epsilon}{(\Delta z)_k}, \quad \varepsilon=\pm 1,\end{cases} \tag{63}$$

$$\begin{cases}\boldsymbol{C}^h_{(i,j+\frac{1}{2},k+\frac{\varepsilon}{2}),\,(i,j+\frac{1}{2},k)} &= \dfrac{\epsilon}{(\Delta z)_k}, \quad \varepsilon=\pm 1,\\ \boldsymbol{C}^h_{(i+\frac{\varepsilon}{2},j+\frac{1}{2},ki),\,(i,j+\frac{1}{2},k)} &= -\dfrac{\epsilon}{(\Delta x)_i}, \quad \varepsilon=\pm 1,\end{cases} \tag{64}$$

and

$$\begin{cases}\boldsymbol{C}^h_{(i+\frac{\varepsilon}{2},j,k+\frac{1}{2}),\,(i,j,k+\frac{1}{2})} &= \dfrac{\epsilon}{(\Delta x)_i}, \quad \varepsilon=\pm 1,\\ \mathbf{C^h}_{(i,j+\frac{\varepsilon}{2},k+\frac{1}{2}),\,(i,j,k+\frac{1}{2})} &= -\dfrac{\epsilon}{(\Delta y)_j}, \quad \varepsilon=\pm 1.\end{cases} \tag{65}$$

5.4 The "stiffness" matrix

The "stiffness" matrix is the symmetric matrix $\boldsymbol{K}$ given by

$$\boldsymbol{K}^h_{e,e'} = \int_\Omega \frac{1}{\mu_0}(\nabla\times\boldsymbol{\phi}_e)\cdot(\nabla\times\boldsymbol{\phi}_{e'})\,dV. \tag{66}$$

Using (62), we get the formulas

$$\begin{aligned}\boldsymbol{K}^h_{e,e'} &= \int_\Omega \frac{1}{\mu_0}\sum_{f_1}\boldsymbol{C}^h_{f_1,a}\boldsymbol{\psi}_{f_1}(\boldsymbol{x})\cdot\sum_{f_2}\boldsymbol{C}^h_{f_2,e'}\boldsymbol{\psi}_{f_2}(\boldsymbol{x})\,dV\\ &= \sum_{f_1}\sum_{f_2}\boldsymbol{C}^h_{f_1,a}\boldsymbol{C}^h_{f_2,e'}\int_\Omega\frac{1}{\mu_0}\boldsymbol{\psi}_{f_1}(\boldsymbol{x})\cdot\boldsymbol{\psi}_{f_2}(\boldsymbol{x})\,dV\\ &= \sum_f \boldsymbol{C}^h_{f,e}\left(\boldsymbol{M}^h_{\frac{1}{\mu_0}}\right)_{f,f}\boldsymbol{C}^h_{f,e'},\end{aligned}$$

where the last equality holds because the mass matrix is diagonal. It is then found that

$$\boldsymbol{K}^h = \left(\boldsymbol{C}^h\right)^T\boldsymbol{M}^h_{\frac{1}{\mu_0}}\,\boldsymbol{C}^h, \tag{67}$$

(superscript T denotes transpose).

5.5 The right hand side

The right hand side of (53) can be split into two terms

$$\boldsymbol{F}_e^h(t) = \boldsymbol{F}_e^{h,m}(t) + \mathbf{F}_e^{h,st}(t), \tag{68}$$

with

$$\left\{ \begin{array}{rcl} \boldsymbol{F}_e^{h,m}(t) & = & \displaystyle\int_\Omega \mathcal{M}_h(\boldsymbol{x},t)\cdot(\nabla\times\boldsymbol{\phi}_e)(\boldsymbol{x})\,dV. \\ \mathbf{F}_e^{h,st}(t) & = & \displaystyle\frac{d}{dt}\int_\Omega \sigma(\boldsymbol{x})\boldsymbol{A}_{s,h}(\boldsymbol{x},t)\cdot\boldsymbol{\phi}_e(\boldsymbol{x})\,dV. \end{array} \right. \tag{69}$$

where, as mentioned before, the fields $\mathcal{M}$ and $\boldsymbol{A}_s$ are approximated in $(\mathcal{H}_h)^3$ and $\mathcal{H}_h^{\rm curl}$ respectively. Th following two paragraphs are devoted to the assembly of those two terms.

5.5.1 The term associated with the magnetic moment

This term uses a new coupling array $\vec{\boldsymbol{\Xi}}^h$ which is an array of vectors. It is readily seen that

$$\boldsymbol{F}_e^{h,m}(t) = \int_\Omega \mathcal{M}_h(\boldsymbol{x},t)\cdot\left(\sum_f \boldsymbol{C}_{f,e}\,\boldsymbol{\phi}_e(\boldsymbol{x})\,d\boldsymbol{x}\right)$$

or, see (39),

$$\boldsymbol{F}_e^{h,m}(t) = \sum_f \boldsymbol{C}_{f,e}\sum_c (\vec{\boldsymbol{\Xi}}_{c,f}\cdot\mathcal{M}_c(t)) \tag{70}$$

where $\mathcal{M}_c = \mathcal{M}_h|_c$ and we have introduced a coupling sparse array $\vec{\boldsymbol{\Xi}}^h$ whose non zero vectorial elements are

$$\left\{ \begin{array}{rcl} \boldsymbol{\Xi}_{(i+\frac{\varepsilon}{2},j+\frac12,k+\frac12),(i,j+\frac12,k+\frac12)} & = & \displaystyle\frac{\hat{\boldsymbol{x}}}{2}\,(\Delta x)_{i+\frac{\varepsilon}{2}}\,(\Delta y)_{j+\frac12}\,(\Delta z)_{k+\frac12},\ \varepsilon=\pm1 \\ \boldsymbol{\Xi}_{(i+\frac12,j+\frac{\varepsilon}{2},k+\frac12),(i+\frac12,j,k+\frac12)} & = & \displaystyle\frac{\hat{\boldsymbol{y}}}{2}\,(\Delta x)_{i+\frac12}\,(\Delta y)_{j+\frac{\varepsilon}{2}}\,(\Delta z)_{k+\frac12},\ \varepsilon=\pm1 \\ \boldsymbol{\Xi}_{(i+\frac12,j+\frac12,k+\frac{\varepsilon}{2}),(i+\frac12,j+\frac12,k)} & = & \displaystyle\frac{\hat{\boldsymbol{z}}}{2}\,(\Delta x)_{i+\frac12}\,(\Delta y)_{j+\frac12}\,(\Delta z)_{k+\frac{\varepsilon}{2}},\ \varepsilon=\pm1. \end{array} \right. \tag{71}$$

Thus, we have

$$\boldsymbol{F}^{h,m}(t) = \left(\boldsymbol{C}^h\right)^T\,\vec{\boldsymbol{\Xi}}^h\cdot\mathcal{M}_h(t) \tag{72}$$

after suitably interpreting the term $\vec{\boldsymbol{\Xi}}^h\cdot\mathcal{M}_h(t)$ using (70).

5.5.2 The right hand side associated with the potential $\boldsymbol{A}_s$

Here, we show how to approximate $\boldsymbol{A}_s$. We assume that the source potential is created by a coil surrounding the heterogeneous part of the medium. More precisely, let $\mathcal{C}oil$ denote some piecewise smooth curve of the space, $I(t)$ some current flowing across the coil; we define $\boldsymbol{A}_s(\boldsymbol{x},t)$ as

$$\boldsymbol{A}_s(\boldsymbol{x},t) = I(t)\,\tilde{\boldsymbol{a}}_s(\boldsymbol{x}).$$

where $\tilde{\boldsymbol{a}}_s(\boldsymbol{x})$ is the solution of the static problem

$$\left\{ \begin{array}{ll} \nabla\times(\nabla\times\tilde{\boldsymbol{a}}_s) = -\mu_0\,\vec{\mu}_{\mathcal{C}oil} & \text{in } \Omega, \\ \tilde{\boldsymbol{a}}_s\times\nu = 0 & \text{on } \partial\Omega. \end{array} \right. \tag{73}$$

Here $\vec{\mu}_{\mathcal{C}oil}$ is the vectorial distribution given by

$$< \vec{\mu}_{\mathcal{C}oil},\, \vec{f} >_{\mathcal{D},\mathcal{D}'} = \int_{\mathcal{C}oil} \vec{f}(\boldsymbol{y}) \cdot d\boldsymbol{s}(\boldsymbol{y}).$$

If the boundary of Ω is far enough from the coil, we get

$$\tilde{\boldsymbol{a}}_s(\boldsymbol{x}) \approx \boldsymbol{a}_s(\boldsymbol{x}) = \frac{\mu_0}{4\pi} \int_{\mathcal{C}oil} \frac{d\boldsymbol{s}(\boldsymbol{y})}{|\boldsymbol{x}-\boldsymbol{y}|}.$$

One way to approximate $\boldsymbol{A}_s$ according to (26) consists in defining,

$$\boldsymbol{A}_{s,h}(\boldsymbol{x},t) = I(t)\; \boldsymbol{a}_{s,h}(\boldsymbol{x}),$$

where $\boldsymbol{a}_{s,h}$ is the approximation of the static field $\boldsymbol{a}_s$ that provides identical circulations along every edges of the mesh. We get

$$\boldsymbol{a}_{s,h}(\boldsymbol{x}) = \sum_e (a_s)_e\; \boldsymbol{\phi}_e(\boldsymbol{x}), \tag{74}$$

where the summation runs over the edges, and

$$(a_s)_e = \frac{1}{|e|} \int_e a_s(\boldsymbol{x}) \cdot d\boldsymbol{x} = \frac{\mu_0}{4\pi|e|} \int_e \left(\int_{\mathcal{C}oil} \frac{d\boldsymbol{s}(\boldsymbol{y})}{|\boldsymbol{x}-\boldsymbol{y}|} \right) \cdot d\boldsymbol{s}(\boldsymbol{x}). \tag{75}$$

($|e|$ is the length of edge e).

To go further, we assume that the coil is approximated by segments

$$\mathcal{C}oil = \bigcup_s \mathcal{C}_s,\; \mathcal{C}_s = [A_s, B_s],$$

in which case, we get

$$(a_s)_e = \frac{\mu_0}{4\pi|e|} \sum_s \int_e \int_{\mathcal{C}_s} \frac{d\boldsymbol{s}(\boldsymbol{x}) \cdot d\boldsymbol{s}(\boldsymbol{y})}{|\boldsymbol{x}-\boldsymbol{y}|} = \frac{\mu_0}{4\pi|e|} \sum_s \mathcal{I}(e,[A_s,B_s])\; \hat{\tau}_e \cdot \hat{\tau}_{[A_s,B_s]}, \tag{76}$$

$\hat{\tau}_\cdot$ is a unit tangential vector, while $\mathcal{I}$ is the scalar quantity

$$\mathcal{I}(s_1,s_2) = \int_{s_1} \int_{s_2} \frac{d\boldsymbol{x} \cdot \hat{\tau}_{s_1}\, d\boldsymbol{y} \cdot \hat{\tau}_{s_2}}{|\boldsymbol{x}-\boldsymbol{y}|}.$$

Now, it is easy to summarise. If we gather the components of $\boldsymbol{a}_{s,h}$, i,e. the (a_s)'s, into a vector $\vec{a}_s$, we obtain simply

$$\boldsymbol{F}_e^{h,st}(t) = \frac{dI(t)}{dt}\; \boldsymbol{M}_1^h\, \vec{a}_s. \tag{77}$$

5.6 Solving the static initial problem

We now need to show how to compute an approximation to $\boldsymbol{M}_0^{\text{div free}}$. This will complete our discussion of the eddy-current/LLG algorithm.

5.6.1 The discrete variational formulation

Let $\boldsymbol{M}_{0,h} \in \mathcal{H}_h^3$ be a given initial magnetisation field. We consider the problem of computing $\boldsymbol{M}_{0,h}^{\text{div free}} \in \mathcal{H}_h^{\text{div}}$ and $Q_h \in \mathcal{H}_h$ such that

$$\left\{ \begin{array}{rcl} \displaystyle\int_\Omega \boldsymbol{M}_{0,h} \cdot \boldsymbol{\psi}_h\, dV & = & \displaystyle\int_\Omega \boldsymbol{M}_{0,h}^{\text{div free}} \cdot \boldsymbol{\psi}_h\, dV + \int_\Omega \nabla \cdot \boldsymbol{\psi}_h\, Q_h\, dV, \\ 0 & = & \displaystyle\int_\Omega \nabla \cdot \boldsymbol{M}_{0,h}^{\text{div free}}\, \xi_h dV, \end{array} \right. \tag{78}$$

for all $\boldsymbol{\psi}_h \in \mathcal{H}_h^{\mathrm{div}}$ and for all $\xi_h \in \mathcal{H}_h$.

To understand how this variational formulation constructs an appropriate discrete $\boldsymbol{M}_{0,h}^{\mathrm{div\,free}}$, note that the second equation above implies that $\nabla \cdot \boldsymbol{M}_{0,h}^{\mathrm{div\,free}} = 0$. Then let us take $\boldsymbol{\psi}_h = \nabla \times \boldsymbol{\phi}_h$, where $\boldsymbol{\phi}_h$ is an arbitrary test function in X_h. Since $\nabla \cdot (\nabla \times \boldsymbol{\phi}_h) = 0$, we get

$$\fint_\Omega \boldsymbol{M}_{0,h} \cdot \nabla \times \boldsymbol{\phi}_f \, dV = \fint_\Omega \boldsymbol{M}_{0,h}^{\mathrm{div\,free}} \cdot \nabla \times \boldsymbol{\phi}_h \, dV.$$

5.6.2 The matrix form of (78)

We now introduce the matrices necessary for solving (78).

- The mass matrix for face functions

$$\left(\mathbf{M}_1^h\right)_{f,f'} = \fint_\Omega \boldsymbol{\psi}_f^h \cdot \boldsymbol{\psi}_{f'}^h \, dV$$

  where f and f' denote some face index. Thanks to the numerical quadrature this matrix is diagonal and we have computed it's entries in Section 5.2.

- The divergence matrix for face functions

$$\left(\mathbf{Div}^h\right)_{c,f'} = \fint_\Omega \chi_c^h \, \nabla \cdot \boldsymbol{\psi}_{f'}^h \, dV$$

  where c denotes some cube and f' some face.

- The coupling array between face functions and vectorial cube functions

$$\left(\vec{\mathbf{\Pi}}^h\right)_{f,c'} = \fint_\Omega \boldsymbol{\psi}_f^h \, \chi_{c'}^h \, dV.$$

  Note that each element of $\vec{\mathbf{\Pi}}^h$ is a vector and the action of this "matrix" is as defined in (70).

To write (78) as a matrix equation we next introduce the vectors of degrees of freedom $\vec{Q} \equiv (Q_c)_{c,\,cube}$, $\vec{M}_0 \equiv (\vec{M}_{0,c})_{c,\,cube}$, and $\vec{M}_0^{\mathrm{div\,free}} \equiv (M_{0,f}^{\mathrm{div\,free}})_{f,\,face}$ which are defined via the representations

$$Q_h(\boldsymbol{x}) = \sum_c Q_c \, \chi_c(\boldsymbol{x}), \qquad (\boldsymbol{M}_{0,h})(\boldsymbol{x}) = \sum_c \vec{M}_{0,c} \, \chi_c(\boldsymbol{x}),$$

$$\vec{\mathbf{M}}_{0,h}^{\mathrm{div\,free}}(\boldsymbol{x}) = \sum_f M_{0,f}^{\mathrm{div\,free}} \, \boldsymbol{\psi}_f^h(\boldsymbol{x}).$$

The system (78) can then be written as

$$\begin{cases} \vec{\mathbf{\Pi}}^h \cdot \vec{M}_0 &= \boldsymbol{M}_1^h \, \vec{M}_0^{\mathrm{div\,free}} &+ \left(\mathbf{Div}^h\right)^T Q, \\ 0 &= \mathbf{Div}^h \vec{M}_0^{\mathrm{div\,free}}, \end{cases}$$

where $\left(\mathbf{Div}^h\right)^T$ is the transpose of $\mathbf{Div}^h$. This may be rewritten as

$$\begin{cases} M_0^{\mathrm{div\,free}} = \left(\mathbf{M}_1^h\right)^{-1} \vec{\mathbf{\Pi}}^h \cdot \vec{M}_0 - \left(\mathbf{M}^h\right)^{-1} \left(\mathbf{Div}^h\right)^T \vec{Q}, \\ \mathbf{Div}^h \left(\left(\mathbf{M}_1^h\right)^{-1} \vec{\mathbf{\Pi}}^h \cdot \vec{M}_0\right) = \mathbf{Div}^h \left(\mathbf{M}^h\right)^{-1} \left(\mathbf{Div}^h\right)^T \vec{Q}, \end{cases}$$

where we recall that $\mathbf{M}_1^h$ is diagonal so it can be inverted easily. Introducing a new variable $\vec{M}_h^{\text{face}}$, this is is equivalent to

$$\begin{cases} \vec{M}_0^{\text{face}} = \left(\mathbf{M}_1^h\right)^{-1} \vec{\mathbf{\Pi}}^h \cdot \vec{M}_0, \\ \mathbf{Div}^h \left(\mathbf{M}_1^h\right)^{-1} \left(\mathbf{Div}^h\right)^T Q = \mathbf{Div}^h \vec{M}_0^{\text{face}}, \\ \vec{M}_0^{\text{div free}} = \vec{M}_0^{\text{face}} - \left(\mathbf{M}_1^h\right)^{-1} \left(\mathbf{Div}^h\right)^T \vec{Q}. \end{cases} \tag{79}$$

Thus we see that it suffices to solve the middle equation of (79) to compute $\vec{M}_0^{\text{div free}}$ which is equivalent to solving Poisson's equation. We next summarise how to compute the various matrices.

5.6.3 Assembly of the system

We have already seen in Section 5.2 how to compute $\mathbf{M}_1^h$. The matrix of vectors $\vec{\mathbf{\Pi}}^h$ is sparse. The only non zero elements are

$$\left(\vec{\mathbf{\Pi}}^h\right)_{(i,j+\frac{1}{2},k+\frac{1}{2}),(i+\frac{\varepsilon}{2},j+\frac{1}{2},k+\frac{1}{2})} = \frac{1}{2}\Delta x_{i+\frac{\varepsilon}{2}} \Delta y_{j+\frac{1}{2}} \Delta z_{k+\frac{1}{2}}\, \hat{x},\ \varepsilon = \pm 1$$

$$\left(\vec{\mathbf{\Pi}}^h\right)_{(i+\frac{1}{2},j,k+\frac{1}{2}),(i+\frac{1}{2},j+\frac{\varepsilon}{2},k+\frac{1}{2})} = \frac{1}{2}\Delta x_{i+\frac{1}{2}} \Delta y_{i+\frac{\varepsilon}{2}} \Delta z_{k+\frac{1}{2}}\, \hat{y},\ \varepsilon = \pm 1$$

$$\left(\vec{\mathbf{\Pi}}^h\right)_{(i+\frac{1}{2},j+\frac{1}{2},k),(i+\frac{1}{2},j+\frac{1}{2},k+\frac{\varepsilon}{2})} = \frac{1}{2}\Delta x_{i+\frac{1}{2}} \Delta y_{i+\frac{1}{2}} \Delta z_{k+\frac{\varepsilon}{2}}\, \hat{z},\ \varepsilon = \pm 1$$

and, it is readily found that

$$\begin{aligned} \left(M_0^{\text{face}}\right)_{i,j+\frac{1}{2},k+\frac{1}{2}} &= \frac{\Delta x_{i+\frac{1}{2}}}{\Delta x_{i+\frac{1}{2}} + \Delta x_{i-\frac{1}{2}}} \vec{M}_{0,(i+\frac{1}{2},j+\frac{1}{2},k+\frac{1}{2})} \cdot \hat{x} \\ &\quad + \frac{\Delta x_{i-\frac{1}{2}}}{\Delta x_{i+\frac{1}{2}} + \Delta x_{i-\frac{1}{2}}} \vec{M}_{0,(i-\frac{1}{2},j+\frac{1}{2},k+\frac{1}{2})} \cdot \hat{x} \\ \left(M_0^{\text{face}}\right)_{i+\frac{1}{2},j,k+\frac{1}{2}} &= \frac{\Delta y_{j+\frac{1}{2}}}{\Delta y_{j+\frac{1}{2}} + \Delta y_{j-\frac{1}{2}}} \vec{M}_{0,(i+\frac{1}{2},j+\frac{1}{2},k+\frac{1}{2})} \cdot \hat{y} \\ &\quad + \frac{\Delta y_{j-\frac{1}{2}}}{\Delta y_{j+\frac{1}{2}} + \Delta y_{j-\frac{1}{2}}} \vec{M}_{0,(i+\frac{1}{2},j-\frac{1}{2},k+\frac{1}{2})} \cdot \hat{y} \\ \left(M_0^{\text{face}}\right)_{i+\frac{1}{2},j+\frac{1}{2},k} &= \frac{\Delta z_{i+\frac{1}{2}}}{\Delta z_{i+\frac{1}{2}} + \Delta z_{i-\frac{1}{2}}} \vec{M}_{0,(i+\frac{1}{2},j+\frac{1}{2},k+\frac{1}{2})} \cdot \hat{z} \\ &\quad + \frac{\Delta z_{k-\frac{1}{2}}}{\Delta z_{k+\frac{1}{2}} + \Delta z_{k-\frac{1}{2}}} \vec{M}_{0,(i+\frac{1}{2},j+\frac{1}{2},k-\frac{1}{2})} \cdot \hat{z} \end{aligned}$$

Having computed $\vec{M}_0^{\text{face}}$ we need to compute $\mathbf{Div}^h$ explicitly. Obviously $\mathbf{Div}^h$ is a matrix sparse. The non zero elements are

$$\begin{cases} \left(\mathbf{Div}^h\right)_{(i+\frac{\varepsilon}{2},j+\frac{1}{2},k+\frac{1}{2}),(i,j+\frac{1}{2},k+\frac{1}{2})} = -\varepsilon\, \Delta y_{j+\frac{1}{2}} \Delta z_{k+\frac{1}{2}},\ \varepsilon = \pm 1 \\ \left(\mathbf{Div}^h\right)_{(i+\frac{1}{2},j+\frac{\varepsilon}{2},k+\frac{1}{2}),(i,j+\frac{1}{2},k+\frac{1}{2})} = -\varepsilon\, \Delta z_{k+\frac{1}{2}} \Delta x_{i+\frac{1}{2}},\ \varepsilon = \pm 1 \\ \left(\mathbf{Div}^h\right)_{(i+\frac{1}{2},j+\frac{1}{2},k+\frac{\varepsilon}{2}),(i,j+\frac{1}{2},k+\frac{1}{2})} = -\varepsilon\, \Delta x_{i+\frac{1}{2}} \Delta y_{j+\frac{1}{2}},\ \varepsilon = \pm 1 \end{cases}$$

and, in particular

$$\left\{\begin{array}{l} \left(\mathbf{Div}^h M_0^{\text{face}}\right)_{i+\frac{1}{2},j+\frac{1}{2},k+\frac{1}{2}} = \\ \Delta y_{j+\frac{1}{2}}\Delta z_{k+\frac{1}{2}}\left(\left(M_0^{\text{face}}\right)_{i+1,j+\frac{1}{2},k+\frac{1}{2}} - \left(M_0^{\text{face}}\right)_{i,j+\frac{1}{2},k+\frac{1}{2}}\right) \\ \Delta z_{k+\frac{1}{2}}\Delta x_{i+\frac{1}{2}}\left(\left(M_0^{\text{face}}\right)_{i+\frac{1}{2},j+1,k+\frac{1}{2}} - \left(M_0^{\text{face}}\right)_{i+\frac{1}{2},j,k+\frac{1}{2}}\right) \\ \Delta x_{i+\frac{1}{2}}\Delta y_{j+\frac{1}{2}}\left(\left(M_0^{\text{face}}\right)_{i+\frac{1}{2},j+\frac{1}{2},k+1} - \left(M_0^{\text{face}}\right)_{i+\frac{1}{2},j+\frac{1}{2},k}\right) \end{array}\right.$$

In order to solve the Poisson problem in (78) we need to form the matrix

$$\mathbf{\Lambda}^h = \mathbf{Div}^h \left(\mathbf{M}^h\right)^{-1} \left(\mathbf{Div}^h\right)^*$$

If we use the previous formulae with the definition of $\mathbf{Div}^h$, we get

$$\begin{aligned} &\left(\mathbf{\Lambda^h} Q\right)_{i+\frac{1}{2},j+\frac{1}{2},k+\frac{1}{2}} = \\ \Delta y_{j+\frac{1}{2}}\Delta z_{k+\frac{1}{2}} \quad &\left(\frac{-2}{\Delta x_{i+\frac{3}{2}} + \Delta x_{i+\frac{1}{2}}}\left(Q_{i+\frac{3}{2},j+\frac{1}{2},k+\frac{1}{2}} - Q_{i+\frac{1}{2},j+\frac{1}{2},k+\frac{1}{2}}\right)\right. \\ &\left. -\frac{-2}{\Delta x_{i+\frac{1}{2}} + \Delta x_{i-\frac{1}{2}}}\left(Q_{i+\frac{1}{2},j+\frac{1}{2},k+\frac{1}{2}} - Q_{i-\frac{1}{2},j+\frac{1}{2},k+\frac{1}{2}}\right)\right) \\ +\Delta z_{k+\frac{1}{2}}\Delta x_{i+\frac{1}{2}} \quad &\left(\frac{-2}{\Delta y_{j+\frac{3}{2}} + \Delta y_{j+\frac{1}{2}}}\left(Q_{i+\frac{1}{2},j+\frac{3}{2},k+\frac{1}{2}} - Q_{i+\frac{1}{2},j+\frac{1}{2},k+\frac{1}{2}}\right)\right. \\ &\left. -\frac{-2}{\Delta y_{j+\frac{1}{2}} + \Delta y_{j-\frac{1}{2}}}\left(Q_{i+\frac{1}{2},j+\frac{1}{2},k+\frac{1}{2}} - Q_{i+\frac{1}{2},j-\frac{1}{2},k+\frac{1}{2}}\right)\right) \\ +\Delta x_{i+\frac{1}{2}}\Delta y_{j+\frac{1}{2}} \quad &\left(\frac{-2}{\Delta z_{k+\frac{3}{2}} + \Delta z_{k+\frac{1}{2}}}\left(Q_{i+\frac{1}{2},j+\frac{1}{2},k+\frac{3}{2}} - Q_{i+\frac{1}{2},j+\frac{1}{2},k+\frac{1}{2}}\right)\right. \\ &\left. -\frac{-2}{\Delta z_{k+\frac{1}{2}} + \Delta z_{k-\frac{1}{2}}}\left(Q_{i+\frac{1}{2},j+\frac{1}{2},k+\frac{1}{2}} - Q_{i+\frac{1}{2},j+\frac{1}{2},k-\frac{1}{2}}\right)\right) \end{aligned}$$

The final matrix operation needed is $\left(\mathbf{M}^h\right)^{-1}\left(\mathbf{Div}^h\right)^T \vec{Q}$ Let

$$M_0^{\text{curl free}} = \left(\mathbf{M}^h\right)^{-1}\left(\mathbf{Div}^h\right)^* Q$$

A simple composition of the formulae shows that

$$\left\{\begin{array}{l} \left(M_0^{\text{curl free}}\right)_{i,j+\frac{1}{2},k+\frac{1}{2}} = \dfrac{-2}{\Delta x_{i+\frac{1}{2}} + \Delta x_{i-\frac{1}{2}}}\left(Q_{i+\frac{1}{2},j+\frac{1}{2},k+\frac{1}{2}} - Q_{i-\frac{1}{2},j+\frac{1}{2},k+\frac{1}{2}}\right) \\ \left(M_0^{\text{curl free}}\right)_{i+\frac{1}{2},j,k+\frac{1}{2}} = \dfrac{-2}{\Delta y_{j+\frac{1}{2}} + \Delta y_{j-\frac{1}{2}}}\left(Q_{i+\frac{1}{2},j+\frac{1}{2},k+\frac{1}{2}} - Q_{i+\frac{1}{2},j-\frac{1}{2},k+\frac{1}{2}}\right) \\ \left(M_0^{\text{curl free}}\right)_{i+\frac{1}{2},j+\frac{1}{2},k} = \dfrac{-2}{\Delta z_{k+\frac{1}{2}} + \Delta z_{k-\frac{1}{2}}}\left(Q_{i+\frac{1}{2},j+\frac{1}{2},k+\frac{1}{2}} - Q_{i+\frac{1}{2},j+\frac{1}{2},k-\frac{1}{2}}\right) \end{array}\right.$$

This is just a finite difference formulation of the Laplacian suitable for non-uniform grids and consistent with the other components of the algorithm. The resulting finite difference equations can be solved by a SSOR preconditioned conjugate gradient scheme (although more efficient possibilities exist).

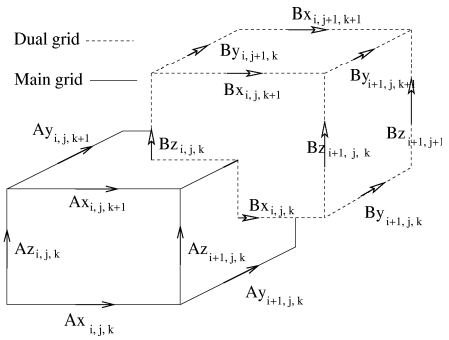

Figure 3: One pair cells of the nonuniform grid G and dual grid $\tilde{G}$

5.7 Comments on the spatial discretization

Once we have completed the assembly procedure we see that the "pseudo mass matrix" $\boldsymbol{M}_\sigma^h$ and the curl-curl matrix $\boldsymbol{K}_h$ are exactly what would be obtained by applying the Finite Integration Technique (see [22] and [6]) to the eddy current model. In this case the arrangement of unknowns is shown in Fig. 3. The right hand side corresponding to the magnetisation is novel, and, as we shall see, allows us to prove an energy conservation result for the semi-discrete scheme.

5.8 Conservation results for the semi-discrete problem

We can now show that (6) holds for the semi-discrete scheme. Choosing $\boldsymbol{\xi}_h = \boldsymbol{M}_h$ on one element c and vanishing on all remaining elements shows that

$$\frac{\partial \boldsymbol{M}_h}{\partial t} \cdot \boldsymbol{M}_h = 0 \text{ on } c$$

where we have used the fact that $\boldsymbol{M}_h$ is constant on c. Thus

$$|\boldsymbol{M}_h| = |\boldsymbol{M}_{0,h}| \quad \text{for all elements } c, \tag{80}$$

where $\boldsymbol{M}_{0,h} \in \mathcal{H}_h^3$ is the discrete initial magnetisation distribution.

The continuous energy balance can also be derived for the semi-discrete system using essentially the same steps. This is possible due to the special choice of spaces for the two fields and the choice of the definition for $\boldsymbol{H}_{\text{eff,h}}$. As in our derivation of the continuous result, we shall assume that $I = 0$. Choosing $\boldsymbol{\phi}_h = \boldsymbol{A}_{h,t} = \partial \boldsymbol{A}_h / \partial t$ in (47) we obtain

$$\oint_\Omega \sigma \boldsymbol{A}_{h,t} \cdot \boldsymbol{A}_{h,t} \, dV = \oint_\Omega \mu_0 \boldsymbol{H}_h \cdot (1/\mu_0) \nabla \times \boldsymbol{A}_{h,t} \, dV.$$

where $\boldsymbol{H}_h = \boldsymbol{M}_{0,h}^{\text{div free}} - \boldsymbol{M}_h - (1/\mu_0)\nabla \times \boldsymbol{A}_h$ since $I = 0$. Expanding the right hand side we obtain

$$\oint_\Omega \sigma \boldsymbol{A}_{h,t} \cdot \boldsymbol{A}_{h,t} \, dV = -\oint_\Omega \mu_0 \boldsymbol{H}_h \cdot \boldsymbol{H}_{h,t} \, dV - \oint_\Omega \mu_0 \boldsymbol{H}_h \cdot \boldsymbol{M}_{h,t} \, dV$$

where we have used the fact that $\partial \boldsymbol{M}_{0,h}^{\text{div free}} / \partial t = 0$. Now using the definition of the effective field

$$\begin{aligned} & \oint_\Omega \sigma \boldsymbol{A}_{h,t} \cdot \boldsymbol{A}_{h,t} \, dV + \oint_\Omega \mu_0 \boldsymbol{H}_h \cdot \boldsymbol{H}_{h,t} \, dV \\ = \quad & -\oint_\Omega \mu_0 \boldsymbol{H}_{\text{eff,h}} \cdot \boldsymbol{M}_{h,t} \, dV - \int_\Omega \mu_0 \left(\frac{2k}{\mu_0} P(\boldsymbol{M}_h) - \frac{2a}{\mu_0} \nabla \cdot \boldsymbol{v}_h \right) \cdot \boldsymbol{M}_{h,t} \, dV. \end{aligned}$$

But using the LLG equation, and noting that $\boldsymbol{H}_{\rm eff,h} \in \mathcal{H}_h^3$ and so can be used as a test function in the discrete LLG equation (51) we obtain

$$\begin{aligned} \fint_\Omega \mu_0 \boldsymbol{H}_{\rm eff,h} \cdot \boldsymbol{M}_{h.t}\, dV &= \fint_\Omega \alpha\mu_0 \left(\boldsymbol{H}_{\rm eff,h} \times \frac{\boldsymbol{M}_h}{|\boldsymbol{M}_h|} \right) \cdot \boldsymbol{M}_{h,t}\, dV \\ &= \fint_\Omega \frac{\mu_0\alpha}{\gamma|\boldsymbol{M}_h|} |\boldsymbol{M}_{h,t}|^2\, dV. \end{aligned}$$

In obtaining this equality we have also used the discrete LLG equation (51) with the test function $\boldsymbol{M}_{h,t}$.

In addition, using the definition of $\boldsymbol{v}_h$ in (49),

$$\fint_\Omega \mu_0 \left(\frac{2k}{\mu_0} P(\boldsymbol{M}_h) - \frac{2a}{\mu_0} \nabla \cdot \boldsymbol{v}_h \right) \cdot \boldsymbol{M}_{h,t}\, dV = \frac{d}{dt} \left(\fint_\Omega k|\boldsymbol{P}(\boldsymbol{M}_h)|^2 + a|\boldsymbol{v}_h|^2 \right) dV.$$

Thus we have proved the following energy equality:

Theorem 2 *Suppose $I = 0$. Then any semi-discrete solution of the the eddy-current LLG equations (47)–(51) satisfies*

$$\begin{aligned} & \frac{d}{dt} \fint_\Omega \left(\frac{1}{2}\mu_0 |\boldsymbol{H}_h|^2 + k|\boldsymbol{P}(\boldsymbol{M}_h)|^2 + a|\boldsymbol{v}_h|^2 \right) dV + \fint_\Omega \sigma |\boldsymbol{A}_{h,t}|^2\, dV \\ = \quad & - \fint_\Omega \frac{\mu_0\alpha}{\gamma|\boldsymbol{M}_h|} |\boldsymbol{M}_{h,t}|^2\, dV. \end{aligned} \tag{81}$$

5.9 Time-stepping

The semi-discrete scheme discussed so far needs to be discretized in time. Let Δt be the size of time step, let $\vec{A}^n$ denoted the unknown degrees of freedom of the vector potential on the edges of the mesh grids at time $t_n = n\Delta t$. In the same way let $\vec{A}_s^n$ denote the vector potential due to the applied field on the edges of the mesh grids at time t_n, and let $\boldsymbol{M}_c^{n+1/2}$ denote the magnetisation $\boldsymbol{M}_h$ at the centre of element c of the mesh at time $t_{n+1/2} = (n + 1/2)\Delta t$, and let $\vec{M}_h$ denote a vector of these vectors.

Using the Crank-Nicholson scheme on equation (53) we obtain (using also the decomposition for $\boldsymbol{K}_h$ in (67)) the fully discrete eddy-current equations

$$\begin{aligned} & M_\sigma^h \frac{A^{n+1} - A^n}{\Delta t} + \boldsymbol{C}^{h,T} \boldsymbol{M}^h_{\frac{1}{\mu_0}} \boldsymbol{C}^h \frac{A^{n+1} + A^n}{2} \\ = \quad & -\frac{dI}{dt}(t^{n+1/2}) M_1^h \boldsymbol{a}_{s,h} - C^{h,T} \vec{\boldsymbol{\Xi}}^h \cdot \vec{M}^{n+1/2}. \end{aligned} \tag{82}$$

where $\vec{\boldsymbol{\Xi}}^h$ is the array mapping the values of magnetisation at the centres of grids to the faces of grids.

At $t_{n+3/2} = (n + 3/2)\Delta t$, the magnetisation is determined by the following equation obtained using the Crank-Nicholson method except for the exchange contribution in $\boldsymbol{H}_{\rm eff,c}$ which is lagged to $t_{n+1/2}$:

$$\begin{aligned} \frac{\boldsymbol{M}_c^{n+3/2} - \boldsymbol{M}_c^{n+1/2}}{\Delta t} &= \gamma \boldsymbol{H}_{\rm eff,c}^{n+1} \times \frac{\boldsymbol{M}_c^{n+3/2} + \boldsymbol{M}_c^{n+1/2}}{2} \\ &\quad + \frac{\alpha}{|\boldsymbol{M}_c|} \frac{\boldsymbol{M}_c^{n+3/2} + \boldsymbol{M}_c^{n+1/2}}{2} \times \frac{\boldsymbol{M}_c^{n+3/2} - \boldsymbol{M}_c^{n+1/2}}{\Delta t} \end{aligned} \tag{83}$$

Recall (50) so that

$$\boldsymbol{H}_{\rm eff,c} = \frac{1}{\mu_0} P_{h,c} \boldsymbol{B}_h + \frac{2a}{\mu_0} \nabla \cdot \boldsymbol{v}_h|_c - \frac{2k}{\mu_0} \boldsymbol{P}(\boldsymbol{M}_c) \tag{84}$$

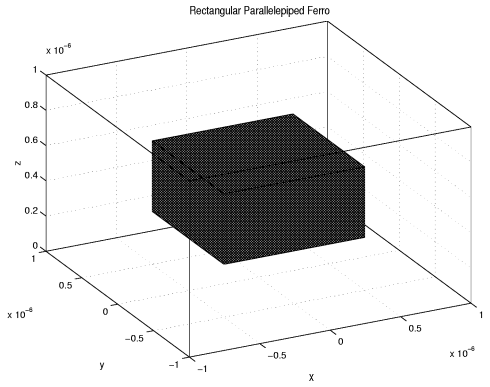

Figure 4: Rectangular parallelepiped ferromagnet. No coil is present and the boundary condition (17) is used on all surfaces of the outer cube.

where $P_{h,c}$ represents the operator averaging the face values of $\boldsymbol{B}_h$ to the centroid of cell c. This leap-frog type scheme has the advantage of conserving the norm of the magnetisation even at the fully discrete level (the electromagnetic energy equality has not been derived for the fully discrete scheme yet). Suppose $\vec{A}^n$ and $\vec{M}^{n+1/2}$ are known, (82) is used to calculate A^{n+1} at t_{n+1}. By (84), we have $H^{n+1}_{\text{eff,c}}$. Finally, (83) is used to obtain $\boldsymbol{M}_c^{n+3/2}$ at $t_{n+3/2}$ for each cell c.

6 Numerical Results

Here we present a few examples of solutions of the eddy current LLG system. One difficulty is to obtain realistic test problems to verify the code. In these examples the eddy current problem is solved at each time step using the SSOR preconditioned conjugate gradient scheme from the NAG library (see also [6]).

6.1 Steady State of a Single Ferromagnet

Test problem 1 has a single rectangular ferromagnet occupying the parallelepiped (dimensions in μm):

$$[-0.5, 0.5] \times [-0.5, 0.5] \times [0.3, 0.7]$$

inside the computational domain (shown in Fig. 5):

$$[-1.0, 1.0] \times [-1.0, 1.0] \times [0.0, 1.0]$$

The domain is decomposed to $20 \times 20 \times 10$ cells. The initial magnetisation is set to $8.0 \times 10^5 A/m$ pointing along $\hat{\boldsymbol{z}}$. There is no applied field and the exchange field is zero, so $a = 0.0 J/m$, $k = 0.0 J/m^3$, $\alpha = 1.2434$, $\Delta t = 5.0 \times 10^{-12} s$, $\gamma = 2.21 \times 10^5$ and $\Delta h \approx 1.0 \times 10^{-7} m$. The boundary condition (17) is enforced on all the boundaries of the computational domain.

While running the code, the magnetic induction $\boldsymbol{B}$ is recorded at different time steps. Fig. 5 is a quiver plot of $\boldsymbol{B}$ on the plane $x_3 = 0.5$ μm. The system finally approaches a plausible steady state as we expect. We have no exact solution to verify this, however.

We have also investigated the effect of changing the damping parameter α on the field. For example, in Fig. 6 we show the magnitude if the magnetic induction $|\boldsymbol{B}|$ at the centre of the cube for various choices of α. As expected, increasing α results in a less oscillatory solution.

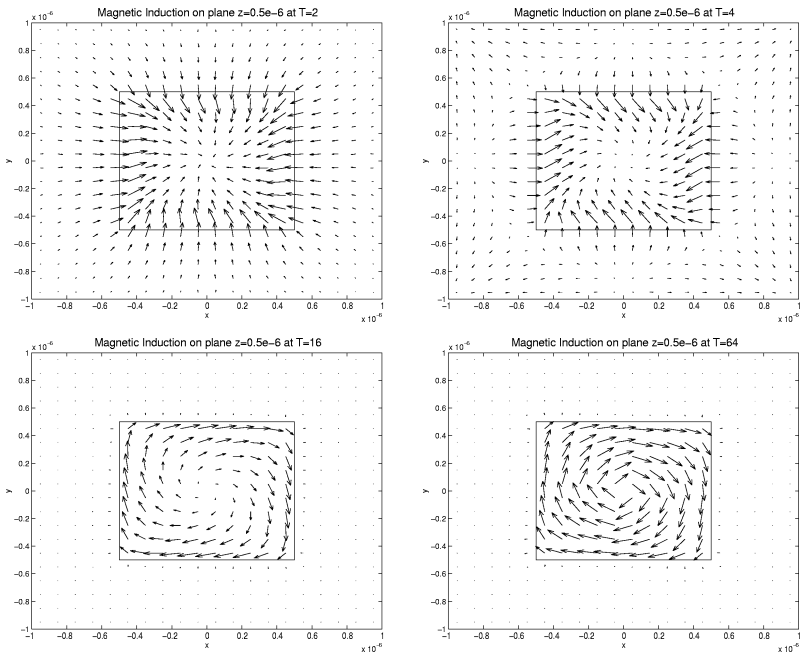

Figure 5: Magnetic Field on plane $z = 0.5\ \mu$m at different time step. This plane cuts through the center of the ferromagnet (in the figure titles, T denotes the number of time steps for the given results).

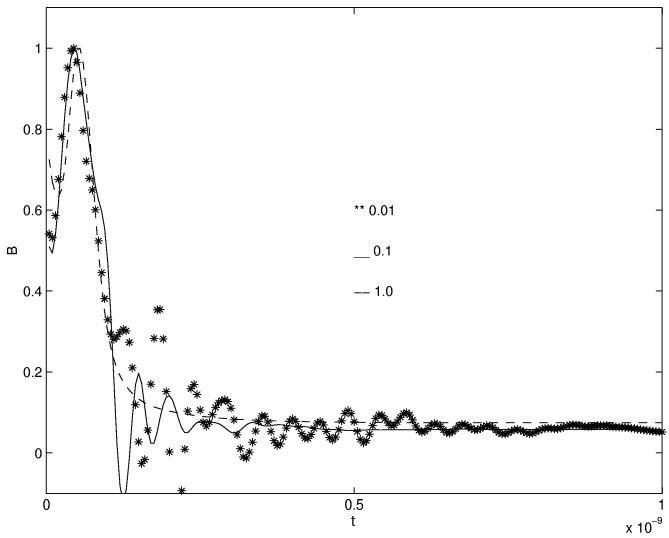

Figure 6: Magnitude of the magnetic induction as a function of time at center of the ferromagnet at different times as the system goes to the steady state. Different α give a different evolution of $|\boldsymbol{B}|$ since increasing α increases the damping in the LLG equation.

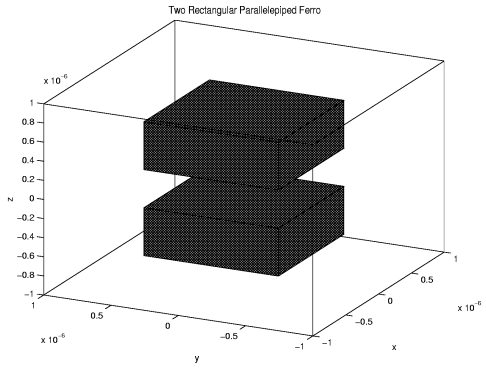

Figure 7: Two rectangular parallelepiped ferromagnets used to test the implementation of the ground plane boundary condition (7).

6.2 Steady State of Two Ferromagnets

Our second test problem is used to test the implementation of the ground plane boundary condition (7). We use two ferromagnets occupying Ω_{ferro} given (in μm) by

$$[-0.5, 0.5] \times [-0.5, 0.5] \times [0.2, 0.7]$$

and

$$[-0.5, 0.5] \times [-0.5, 0.5] \times [-0.2, -0.7]$$

inside the computational domain Ω given by (see Fig. 7):

$$[-1.0, 1.0] \times [-1.0, 1.0] \times [-1.0, 1.0].$$

The domain is decomposed to $20 \times 20 \times 20$ cells. The initial magnetisation is set to point along $\hat{\boldsymbol{x}}$ in one ferromagnet and the $-\hat{\boldsymbol{x}}$ direction in another. The boundary condition (17) is applied on the boundary of the entire computational domain. There is no applied field. and the exchange field is zero, so $a = 0.0J/m$, $k = 0.0J/m^3$, $\alpha = 1.2434$, $\Delta t = 5.0 \times 10^{-12}s$, $\gamma = 2.21 \times 10^5$ and $\Delta h \approx 1.0 \times 10^{-7}m$. The magnetic induction is plotted at different time steps in the same way as for test problem 1. The system approaches a steady state after some time and this is shown in Fig. 8 (compared to Fig. 5, the influence of the two ferromagnets in the magnetisation is obvious).

This case can be used to verify the code for the infinite permeability condition (7) at $z = 0$. A second numerical test is performed by computing using only the upper half of the domain in Fig. 7 with the infinite permeability condition at $z = 0$. As we expect, the magnetic field in Fig. 9 is the same as in the upper half in Fig. 8. the numerical results are identical and verify that the boundary condition (7) is correctly implemented at $x_3 = 0$.

6.3 Some results for the Seagate Modal

The academic Seagate perpendicular head model contains a complex ferromagnet consisting of three parallelepipeds (see Fig.10). They are given by (in μm) by

$$[1.0, 2.0] \times [-0.05, 0.05] \times [0.0, 1.0],$$

$$[-1.1, 2.0] \times [-0.05, 0.05] \times [0.5, 1.0],$$

and

$$[-1.1, -1.0] \times [-0.05, 0.05] \times [0.0, 0.5].$$

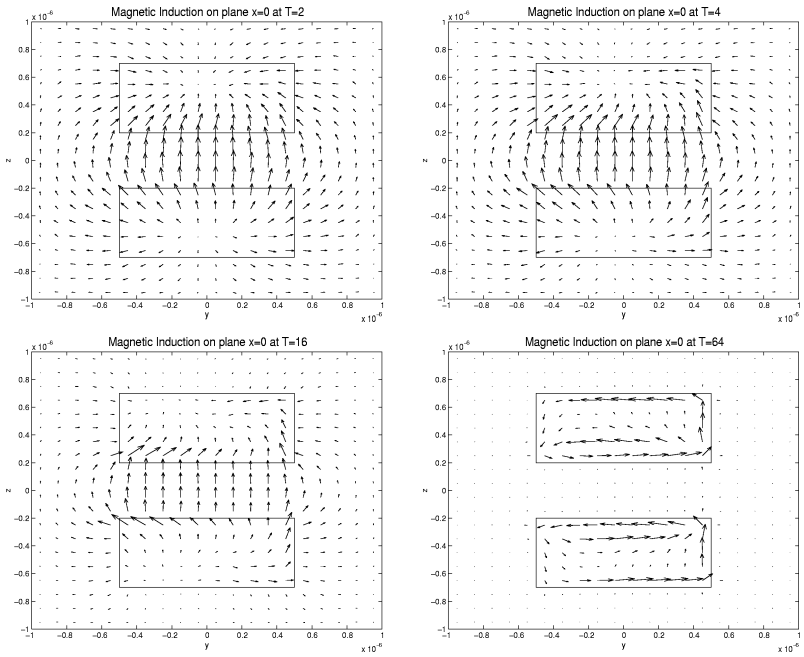

Figure 8: Magnetic induction on plane $x = 0$ at different times for the pair of ferromagnets shown in Fig. 7. Since the initial condition for $\boldsymbol{M}$ is anti-parallel, the solution reflects this asymmetry.

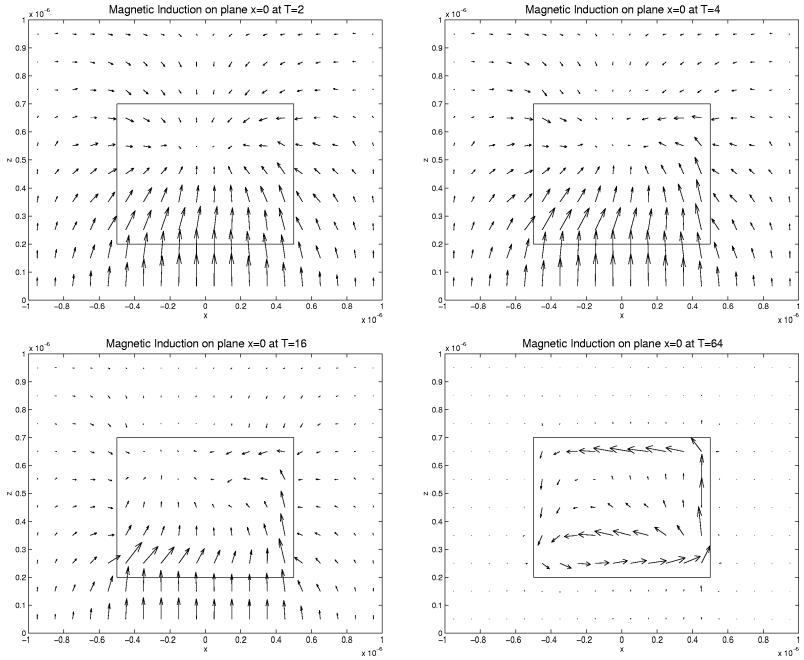

Figure 9: Magnetic induction on plane $x = 0$ at different time steps for the single ferromagnet with the ground plane at $z = 0$ active (corresponding to the upper half of the pair of ferromagnets in Fig. 7). Because the boundary condition (7) imposes an antisymmetry condition on the solution, the solution for this problem is identical to the solution in the upper half of the two magnet problem shown in Fig. 8.

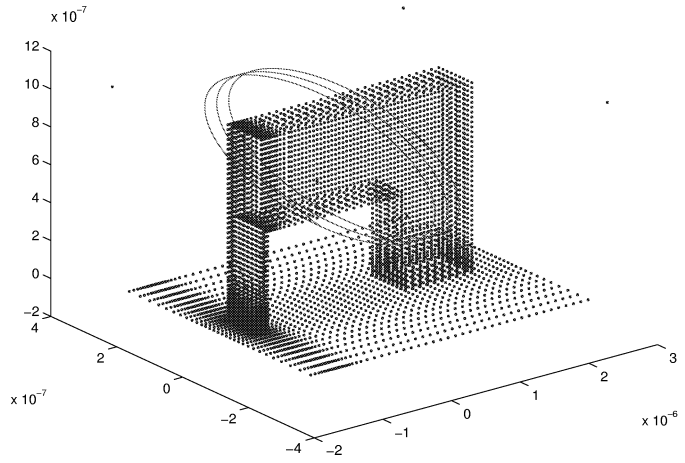

Figure 10: Academic Seagate model showing the distribution of mesh points (vertices of the cubes) on the ferromagnet and on the ground plane. A three turn coil is also shown.

The computational domain is

$$[-1.502, 2.726.0] \quad \times \quad [-0.3048, 0.3173] \times [-0.04, 1.029]$$

A three turn coil is also shown (this does not follow the mesh lines).

The initial magnetisation is set to point in the positive z direction, and there is no initial applied field due to the coils. The domain is decomposed into $60 \times 30 \times 55$ nonuniform cells as shown in Fig. 1. The grid cells around the writing tip are about one tenth of the grid size away from the tip. We choose $a = 1.3 \times 10^{-11} J/m$, $k = 0.0 J/m^3$, $\alpha = 1$, $\Delta t = 1 \times 10^{-12} s$, $\gamma = 2.21 \times 10^5$ and $\Delta h \approx 1.0 \times 10^{-8} m$. The infinite permeability condition is enforced on the ground plane $z = 0$.

At time $t = 0$ the current in the coil rises and creates an applied field. Fig.11 shows a plot of magnetic induction along $\hat{\boldsymbol{z}}$ on the plane $z = 0$ under the writing head at $t = 6 \times 10^{-12}$s (after 6 timesteps). The design of the yoke is such that the magnetic induction under the tip is much higher than under the larger part of the yoke.

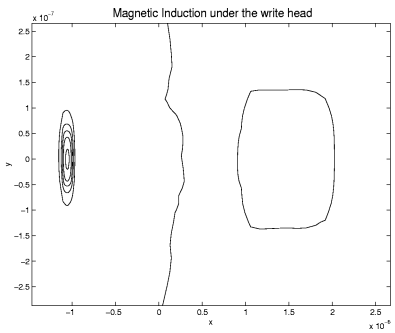

Figure 11: Magnetic induction on the ground plane plane under the write head at time $t = 6 \times 10^{-12}$s.

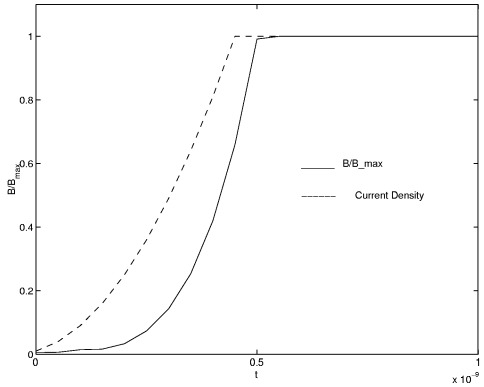

Figure 12: Variation of magnetic induction at the center of the tip against time (solid line). This delays behind the rise of the current in the coil shown as a dashed line.

When the current is turned on, the coil around the ferromagnet generates a magnetic field. The magnetic induction will react to this field. Fig.12 shows the maximum magnetic induction on a plane under the write head and the coil current at different time steps. The magnetic induction lags behind the input current and the lag time is of particular interest for engineers. The lag time is roughly a quarter of nanosecond in this simulation

Figure 13 shows details of the magnetic induction on the mid plane of the writer and some details of the field at the pole tip. Considerable non-uniformity can be seen in the field as the writer is activated.

7 Conclusion

We have presented a model of the perpendicular disc write head that includes eddy current and micromagnetic influences. This is discretized by a simple finite difference method that is adapted to conserve energy. In future we intend to prove convergence of this scheme and verify the method further. In particular the influence of the eddy currents on the field at the pole tip needs to be quantified to verify that eddy current effects are important in the writer.

Perhaps the biggest difficulty with the code is that the eddy current solver is slow due to difficulties in solving the matrix problem resulting from the eddy current discretization. A more advanced multigrid strategy is now under consideration.

Acknowledgements

The research of J. Sun was supported by a grant from Seagate Inc. The research of P. Monk was supported by a grant from AFOSR, and was carried out, in part, during a visit to the Isaac Newton Institute, Cambridge, UK.

References

[1] F. Alouges and A. Soyeur. On global weak solutions for Landau Lifschitz equations: existence and non uniqueness. *Nonlinear Anal., Theory Methods Appl.*, 18:1071–84, 1992.

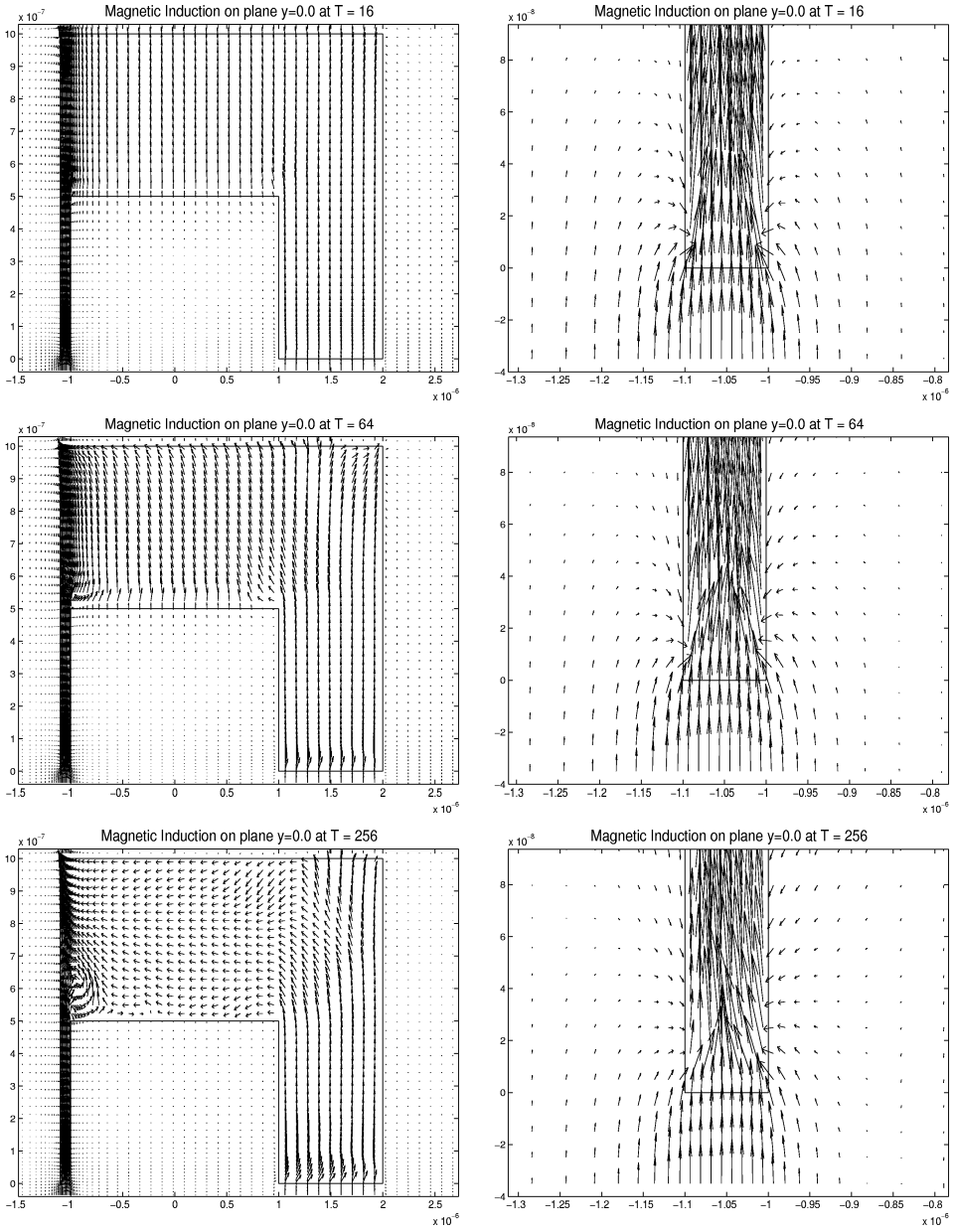

Figure 13: Details of the magnetic induction on the mid plane of the writer and some details of the field at the pole tip. For this example $\Delta t = 1 \times 10^{-12}$s and $\alpha = 1$, and T denotes the number of time steps to the given result.

[2] A.Magni, G.Bertotti, I.D.Mayergoyz, and C.Serpico. Landau-Lifschitz-Gilbert dynamics and eddy current effects in metallic thin films. *J. Magn. Magn. Mat.*, 210:254–5, 2003.

[3] A. Bossavit. Simplicial finite elements for scattering problems in electromagnetism. *Comp. Meth. in Appl. Mech. and Eng.*, 76:299–316, 1989.

[4] W.B. Brown. *Micromagnetics.* Tracts of Physics. Interscience, 1963.

[5] C. Carstensen and A. Prohl. Numerical analysis of relaxed micromagnetics by penalised finite elements. *Numer. Math.*, 90:65–99, 2001.

[6] M. Clemens and T. Weiland. Transient Eddy-Current Calculation with the FI-Method . *IEEE Transactions on Magnetics*, 35:1163–1166, 1999.

[7] W. E and X.-P. Wang. Numerical methods for the Landau-Lifshitz equation. Preprint.

[8] J. Fidler, T. Schrefl, V.D. Tsiantos, W. Scholz, and D. Suess. Micromagnetic simulation of the magnetic switching behaviour of mesoscopic and nanoscopic structures. *Comp. Mat. Sci.*, 24:163–74, 2002.

[9] D. R. Fredkin and T.R. Koehler. Hybrid method for computing demagnetizing fields. *IEEE Trans. Magn.*, 26:415–417, 1990.

[10] A.Magniand G.Bertotti, I.D.Mayergoyz, and C. Serpico. Landau-Lifshitz magnetization dynamics and eddy currents in metallic thin films. *J.Appl.Phys.*, 91:7559, 2002.

[11] B. Lax and K.J. Button. *Microwave ferrites and ferrimagnetics.* McGraw-Hill, 1962.

[12] D. Lewis and N. Nigam. Geometric integration on spheres and some interesting applications. *J. Comput. Appl. Math.*, 151(141-70), 2003.

[13] J.C. Nédélec. Mixed finite elements in $\mathbb{R}^3$. *Numer. Math.*, 35:315–41, 1980.

[14] J.C. Nedelec. A new family of mixed finite elements in r^3. *Num. Math.*, 50:57–81, 1986.

[15] A. Prohl. *Computational Micromagnetism.* Teubner, 2001.

[16] C. Serpico and I.D. Mayergoyz. Analysis of eddy currents with Landau-Lifshitz equation as a constitutive relation. *IEEE Trans. Mag.*, 37:3546–9, 2001.

[17] M. Slodicka and I. Cimrak. Numerical study of nonlinear ferromagnetic materials. Preprint.

[18] A. Taflove. *Computational Electrodynamics.* Artech House, Boston, 1995.

[19] O. Vacus and P. Monk. Accurate discretization of non-linear micromagnetic problem. *Comput. Methods. Appl. Mech. Engrg.*, 190:5243–69, 2001.

[20] A. Visintin. On Landau-Lifchitz' equations for ferromagnetism. *Japan journal of applied mathematics*, 2:69–84, 1985.

[21] X.-P. Wang, C.J. Garcá-Cervera, and W. E. A Gauss Seidel projection method for micromagnetics simulations. *J. Comput. Phys.*, 171:357–72, 2001.

[22] T. Weiland. Time domain electromagnetic field computation with finite difference methods . *International Journal of Numerical Modelling: Electronic Networks, Devices and Fields*, 9:259–319, 1996.

[23] B. Yang and D.R. Fredkin. Dynamical micromagnetics by the finite element method. *IEEE Trans. Mag.*, 34:3842–52, 1998.

[24] K.S. Yee. Numerical solution of initial boundary value problems involving Maxwell's equations in isotropic media . *IEEE Antenna and Propagation*, AP14:302–307, 1966.